ROYAL SOCIETY OF CHEMISTRY

REVIEW

Check for updates

Soft-template-assisted synthesis: a promising approach for the fabrication of transition metal oxides

Rasha Rahman Poolakkandy and Mini Mol Menamparambath [ID] *

The past few decades have witnessed transition metal oxides (TMOs) as promising candidates for a plethora of applications in numerous fields. The exceptional properties retained by these materials have rendered them of paramount emphasis as functional materials. Thus, the controlled and scalable synthesis of transition metal oxides with desired properties has received enormous attention. Out of different top-down and bottom-up approaches, template-assisted synthesis predominates as an adept approach for the facile synthesis of transition metal oxides, owing to its phenomenal ability for morphological and physicochemical tuning. This review presents a comprehensive examination of the recent advances in the soft-template-assisted synthesis of TMOs, focusing on the morphological and physicochemical tuning aided by different soft-templates. The promising applications of TMOs are explained in detail, emphasizing those with excellent performances.

1. Introduction

The advancement of nanotechnology has captivated the perception of researchers for the formulation of cutting-edge materials for varied applications.[1–4] One of the preeminent classes of such materials is transition metal oxides (TMOs), which have been deemed as functional materials over the

Department of Chemistry, National Institute of Technology Calicut, Calicut-673601, Kerala, India. E-mail: neeharabindu@gmail.com; minimol@nitc.ac.in

years.[5–9] The partially filled d-shells of the positive metallic ions in TMOs render them phenomenal properties such as high dielectric constants,[10,11] competent electrical characteristics,[12,13] reactive electronic transitions[14] and broader band gaps.[15,16] These diverse features together with reduced cost, environmental compatibility and easy availability[17] have driven TMOs as a proficient material for a broad spectrum of applications including energy conversion and storage,[17–22] catalysis,[23,24] sensing,[25,26] and bio-based applications.[27,28] The regulation of the structure, morphology, stoichiometry, size and crystallinity

Rasha Rahman Poolakkandy is currently a PhD candidate in the Department of Chemistry, National Institute of Technology, Calicut. She received her Bachelor's degree in Chemistry (2012) from Farook College, Calicut and Master's degree in Chemistry (2015) from St. Joseph's College, Devagiri. Her research interests include the soft-template-assisted synthesis of transition metal oxides and their application in neurotransmitter detection.

Mini Mol Menamparambath is currently an Assistant Professor in the Department of Chemistry, National Institute of Technology Calicut (NITC). She received her PhD in the optoelectronics of single-walled carbon nanotube composites for flexible electronics from Sungkyunkwan University, South Korea in 2014 and continued her post-doctoral research at the same university. She joined NITC in 2016, to work on the development of multi-functional nanomaterials. Her research interests include multi-dimensional nanomaterials, flexible/stretchable nanomaterial polymer composites for applications such as energy production and storage, conductive inks and sensors.

of TMOs greatly control their properties and applications.[29–31] The intricate surface chemistry and the occupancy of lattice vacancies also contribute to their properties by disrupting their electronic arrangement.[32] Hence, continuous efforts have been employed for the controlled and scalable synthesis of TMOs with desired properties.[33–36]

The synthesis of TMOs follows one of two approaches, namely, the top-down approach, or the bottom-up approach. The top-down approach focuses on the curtailing of the magnitude and dimension of the component from the bulk, while the bottom-up approach emphasizes the fabrication of nanomaterials from smaller atoms or molecules.[37] Of the various synthesis pathways, the template-assisted method is an advancing bottom-up approach for the preparation of highly crystalline mesoporous TMOs.[38–41] Template-assisted synthesis methods can be broadly classified as hard-template and soft-template assisted methods,[42] and colloidal templates are an emerging theme in this synthesis strategy.[43] While hard-templates are chiefly inorganic-based,[44] with silica being the most important among them,[45] soft-templates are primarily organic-based, like surfactants, block polymers, or flexible organic molecules.[44,46] In comparison with the hard-templates, soft-templates are favored by virtue of their low cost and easy synthesis without the need for tedious processes for the removal of the template.[46]

This review is intended to give a sketch of the recent progress in the state-of-the-art research that converges on the soft-template-assisted synthesis strategies for TMOs. Though earlier reviews have presented exquisite summaries of various synthesis methods of TMOs[37,47–49] and various template-assisted synthesis approaches,[42,50,51] this review explicitly focuses on the

synthesis of TMOs using soft-templates and their diverse applications. The review opens with a brief description of the general synthesis methods of TMOs, including top-down and bottom-up approaches, and advances with the meticulous examination of template-assisted synthesis methods. Of the various template-assisted synthesis schemes, the soft-template assisted approach is focused on the preparation of TMOs and different soft-templates have been discussed comprehensively by taking into account the distinct property tuning achieved using this method. The promising applications of TMOs are explained in detail, highlighting those with superior performance. An outline of the prevailing research status and development is given, along with the future perspectives and challenges in this upcoming area.

2. General synthesis strategies of TMOs

The fabrication of TMOs with superior properties for peculiar applications is often a tedious effort. The surface instability generated by the strong surface polarization due to the absence of solid interlayer interactions endures as a hurdle for the synthesis of TMOs with specific morphologies.[52] However, these obstacles can be overcome by undertaking pertinent synthesis methods for the preparation of TMOs with notable lattice relaxations and pronounced structural reconstruction.[53,54] For such an effective synthesis, comprehensive insight into the interactions between the precursor materials is required, along with their absolute distribution.[55] The methods for TMO synthesis can be generally sorted into two broad classes: the top-down approach and the bottom-up approach. The schematic
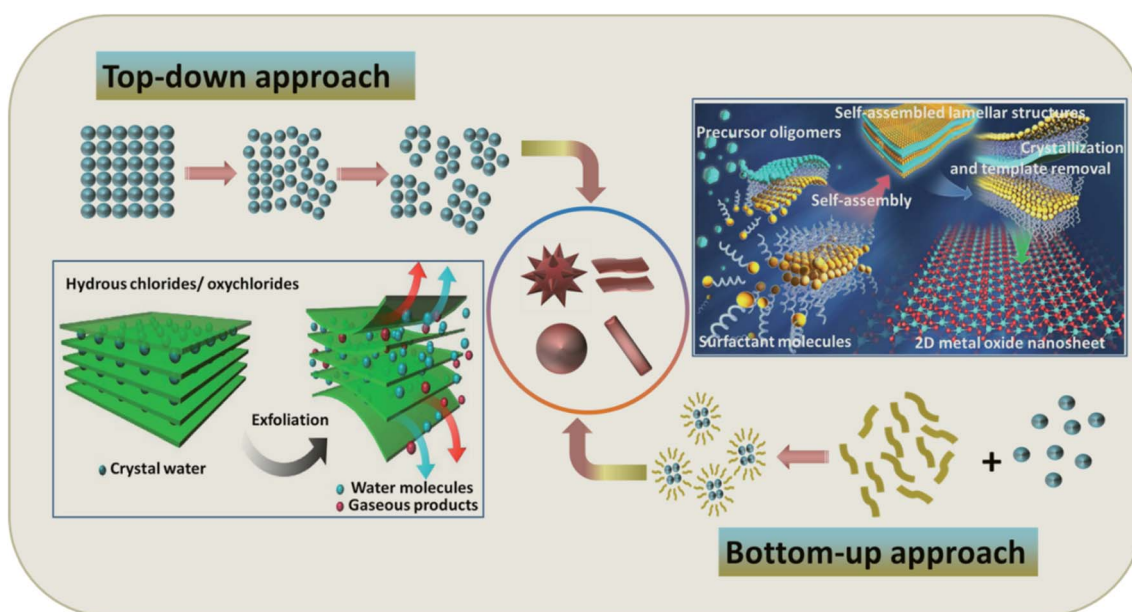

Fig. 1 Schematic representations of the top–down and bottom–up approaches with typical examples: (Bottom left) schematic representation of the exfoliation of hydrous chlorides as an example of the top–down approach. Adapted with permission from ref. 58. Copyright 2016 Springer Nature publishing. (Top right) Schematics for the molecular assembly of ultrathin 2D metal oxide nanosheets as an example of the bottom–up approach. Reproduced with permission from ref. 33. Copyright 2016 Springer Nature publishing.

representations of these methods along with typical examples are provided in Fig. 1. Some of the synthesis methods even follow a combined route of these two approaches, mainly for the synthesis of hybrid materials.[56,57]

The top-down approach mainly implicates reducing the size and dimensions of bulk materials in order to design the targeted products. It makes use of the process of lithography, including physical and chemical etching along with other processes like mechanical milling and exfoliation.[58,59] Being an accessible and efficient route without the demand for complicated methods and equipment, this technique can be employed for comparably large-scale production. Furthermore, the materials synthesized *via* this approach usually retain high crystallinity, which is acquired from the host material.[60] Notwithstanding these advantages, the top-down approach also has its own drawbacks, including the feeble quality distribution of the attained product, broad size distribution and varied sizes and shapes of the products, formation of internal stress, structural defects and deterioration, and most importantly, the requirement of appropriate host materials.[60]

Nature's ability to exploit chemical or physical forces for the creation of self-assembled structures has inspired researchers to mimic this strategy for the preparation of a wide range of materials, giving rise to a new concept of the bottom-up approach. This approach adopts chemical or physical forces driving at the nanoscale to compile basic units into larger structures for multifunctional nanostructure systems and devices.[61] The bottom-up approach affords the utmost limits of miniaturization by offering tunable, cost-effective, and readily controlled processes for the high yield of uniform products. However, the need for complex synthesis steps has limited its application to simple nanostructured materials.[60] The advantages and disadvantages of the top-down and bottom-up approaches are highlighted in Table 1.

The bottom-up approach is further sub-categorized as vapor-based, solution-based and template-based methods.[62] When compared to the vapor deposition and solution-based methods, the template-assisted synthesis is an advancing technique in the bottom-up approach for the controlled synthesis of nanostructures. It is a cost-effective technique capable of regulating the morphology and structure of the nanomaterials for customized applications.[63] The synthesis of highly ordered mesoporous nanostructures is the major highlight of this method.[64] It makes use of a template, which acts as a scaffold for guiding the growth of nanostructures for obtaining different geometries and morphologies.[65] Since the principal focus of this review is the soft-template-assisted synthesis of TMOs, the template-based synthetic approaches are discussed in detail in the forthcoming sections.

3. Template-assisted synthesis of TMOs

The major factor of a template-assisted synthesis is the "template", which can be any entity with nanostructured characteristics, and whose size, morphology and charge dissemination greatly influence the structure guiding properties.[66] The initial step in the template-assisted synthesis is the preparation of the template, followed by the fabrication of the desired material using the template and the elimination of the template, if necessary. The fabrication of the desired material may include physical methods such as surface coating or chemical methods like addition, elimination, substitution, or isomerization reactions. Once the reaction is completed, the template may be eliminated by physical methods like dissolution or chemical methods like calcination.[42] The major benefit of the template-assisted method is its effective control over the structure, dimension and morphology of the end product. Different TMOs with varied morphologies including 1D, 2D and 3D structures have been synthesized using this technique.[67–70] Based on the type of template present, the template-assisted synthesis can be further classified as a hard-template method, soft-template method, or colloidal-template method. A schematic representation of the fabrication of materials using these templates is provided in Fig. 2.

3.1 Hard-template method

The hard-template method, also termed as nanocasting, adopts a solid mold with a well-defined design, whose surfaces or pores are subsequently filled by the precursor molecules to form the final product. Once the reaction is completed, the mold is removed without affecting the properties of the product.[51,71] There are different types of hard-templates like macroscopic structures and *in situ*-formed templates, which can be used for the synthesis processes. Macroscopic structures may consist of fibers, powders, or films. Typical examples are anodized aluminum oxide (AAO),[72,73] biological materials such as organic macromolecules, tissues and biomolecules,[74] polymeric microspheres[75] and silica.[76] *In situ* hard templates refer to the templates formed by the *in situ* physical or chemical conversion of a compound in the precursors. Common examples include ice crystals, salt, or carbon.[77,78] As the structural and morphological features of the acquired product immensely rely on the

Table 1 Advantages and disadvantages of the top-down and bottom-up approaches for the synthesis of TMOs

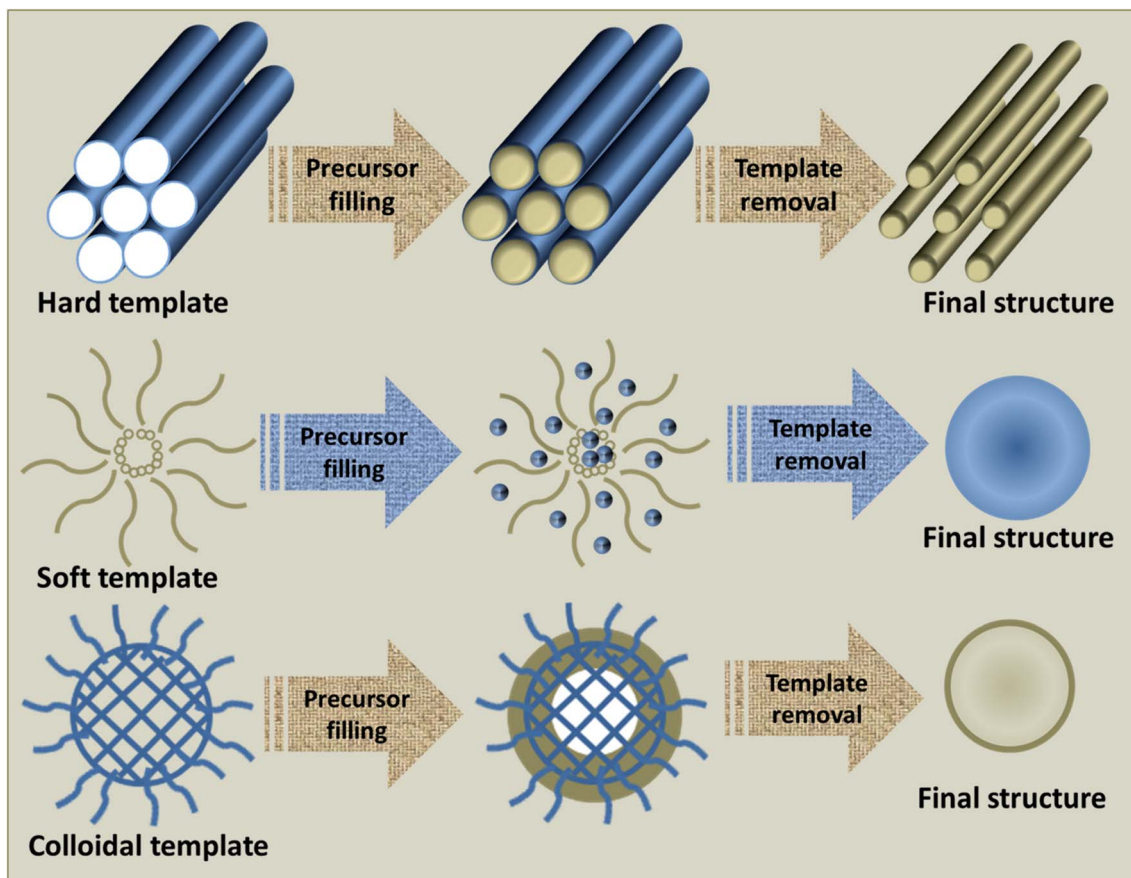| Top-down approach	Bottom-up approach
Advantages	
Employed for the large-scale production of nano/microscale structures	Controlled tuning of the morphology, pore size, crystallinity and phase
Synthesized materials retain high crystallinity	Control of the reaction parameters
Non-requirement of chemical purification	Cost-effective technique
Disadvantages	
Structural defects and deterioration	Complex synthesis steps
Formation of internal stress	Difficult for large-scale production
Feeble morphology distribution of the products	Requires chemical purification

Fig. 2 Schematic representation of the synthesis of materials using different types of templates.

quality and attributes of the template and their interaction with the precursors, a judicious selection of the template is crucial for the fabrication of desired products.[79] Though hard-template-assisted synthesis is a prominent method for the synthesis of crystalline oxides, certain features act as a challenge for its effective utilization. These may include their comparably less controllable pore size, lower yield resulting from the irresistible nucleation occurring outside the pore and their tedious processes with high cost.[80,81]

3.2 Soft-template method

The soft-template method commonly makes use of flexible nanostructures as soft-templates, which are composed by intermolecular interactions. The soft-templates are comprised of soft matter, including surfactants, flexible organic molecules and block copolymers.[82] The interactions of these templates with the precursors normally occurs by weak non-covalent bonds, like electrostatic or van der Waals interactions and hydrogen bonding.[83] Compared with the hard-template methods, soft-template-assisted synthesis imparts immense control on the geometry, morphology and size of the product by virtue of the controlled sol–gel transition of the precursors to their oxides.[84] Since soft-template-assisted synthesis is the core theme of this review, the detailed description of this method

along with its importance in the synthesis of TMOs will be presented in the forthcoming discussions.

3.3 Colloidal-template method

The enhancement of the thermal stability of the polymer-based template and the restriction of the crystal growth during heat treatment are the key challenges faced in the soft-template method, which has led to the introduction of another concept of the colloidal-template. In a colloidal-template, the stability of the template is enhanced by the incorporation of inorganic components into polymer templates for delivering increased thermal stability;[85] hence, it is an inorganic nanoparticle core bound with flexible polymer tails. Here, the polymer part acts as a soft-template for organizing the inorganic particles to form nanostructures *via* self-assembly, whereas the inorganic particles act as hard-template for the enhancement of stability and nanoconfinement for the production of desired materials;[86] thus, the colloidal-templates offer the synergetic features of both soft and hard templates. With the aid of colloidal-templates, ordered nanostructures with remarkable crystallinity and structural integrity with controlled pores have been formed, which can withstand higher calcination temperatures.[87] Moreover, highly crystalline mesoporous materials can be prepared without using thermal treatment by retaining their mesostructure.[88] This method has been employed for the

synthesis of a large number of TMOs nanoparticles and TMOs/noble metal hybrids for diverse applications.[89–92]

4. Soft-template-assisted synthesis of TMOs

In the soft-template assisted synthesis of nanostructures, the inorganic precursor species are deposited on either the surface or the interior of the soft-template by techniques like precipitation, electrochemical methods, or similar routes for composing particles with well-defined sizes and shapes.[93] The soft-template is then removed by low-temperature chemical treatment or pyrolysis for obtaining the desired product.[94]

4.1 The general synthetic strategy of the soft-template method

The addition of the precursor molecule into the soft-template can bring about considerable modifications in the self-assembly process leading to micelle/liquid crystal formation for templating the sol–gel process.[95] This regulation of the sol–gel conversion of the precursors during self-assembly is considered to be the decisive step in soft-template methods. The general steps included in the formation of nanostructures from the soft-template are discussed below and a schematic representation is given in Fig. 3.

4.1.1 Cooperative assembly. The initial step in the soft-template assisted synthesis is the assembly of precursors and templates, which occur concurrently in many of the reactions. This step is termed "cooperative assembly", where small groups of precursors and soft matter held together by the above-mentioned weak intermolecular interactions are formed in the solution, which then integrates into bulkier structures.[94] Eventually, this leads to the development of a liquid-crystalline phase enclosed by the precursors, which precipitates out of the solution. By judiciously governing this cooperative assembly step, the desired product can be obtained by following the processes given below.

4.1.2 Liquid-crystal templating. This method resembles that of hard-template synthesis in that a liquid-crystalline phase is formed, cast around by the inorganic material. This process requires specific parameters such as a high concentration of surfactants, which induces higher viscosity in the solution, thereby limiting its application.[94] Nevertheless, it exists as an appropriate method for the preparation of certain products with precursors like chloroplatinic acid, which are compatible with these viscous solutions.[96]

4.1.3 Evaporation-induced self-assembly (EISA). EISA is one of the most effective methods, especially for the synthesis of metal oxides. It involves three major steps:[97]

(1) Preparation of a dilute solution (sol) consisting of the inorganic/organic precursors, soft-template and a volatile solvent with suitable stoichiometry.

(2) Dispersion of this solution over a vast area to attain the critical micelle concentration by evaporation of the solvent and the self-assembly of the precursors into the micelles owing to their feeble condensation, resulting in a state called a tunable steady state.

(3) Development of the final structure by further inorganic condensation of the precursor around the liquid crystalline phase.

The successful fabrication of the desired final structure is completed by further processing techniques for the removal of the soft-template without affecting the properties of the product. Soft-templates such as surfactants can be eliminated by several methods such as low-temperature chemical treatment, combustion or depolymerization via thermal treatment or calcination.[42] Care should be taken in these steps to retain the properties of the product such as porosity and structure and appropriate methods should be adopted.

4.2 Synthesis of TMOs with a surfactant as the soft-template

Surfactants are amphiphilic molecules consisting of both hydrophobic and hydrophilic counterparts, which lower the surface and interfacial tension. Based on the charge possessed
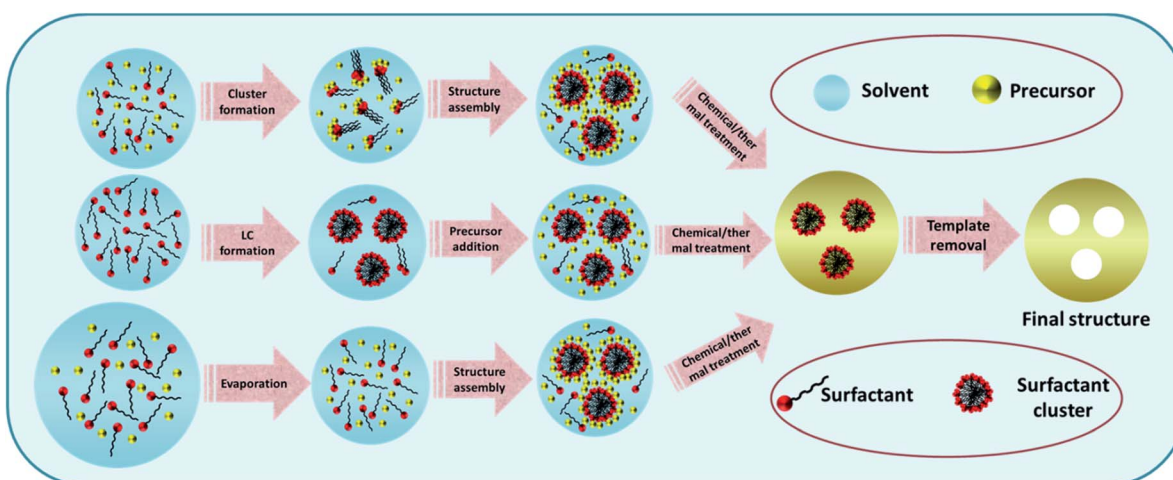

Fig. 3 Schematic representation of the general steps included in the formation of nanostructures using the soft-template: cooperative assembly, liquid crystal (LC) templating and evaporation-induced self-assembly (EISA).

by the head group in neutral solution, surfactants can be broadly classified as ionic (cationic and anionic) and non-ionic surfactants.[95] As ionic surfactants interact with the precursors using electrostatic interactions, the self-assembly processes mediated by non-ionic surfactants are mainly facilitated by van der Waals interactions and hydrogen bonding.[42] The choice of suitable surfactants is the fundamental step for tuning various properties like the structure and pore size of the mesostructures formed.

There are four reported synthetic models for the surfactant-assisted self-assembly. They are S^+I^-, S^-I^+, $S^+X^-I^+$ and $S^-X^+I^-$, where "S" stands for the surfactant, "I" for the inorganic precursor and "X" for the mediator.[98] From these models, it is clear that the modification of the surfactant ionization state is a crucial factor for the synthesis of desired structures. The formation of micelles/liquid-crystals is the most critical part of the soft-templating process. For the successful formation of micelles, the attainment of optimum temperature for the dissolution of the surfactant, called the Krafft temperature, and an optimum concentration of surfactant, called the critical micelle concentration (CMC), are imperative.[99] On satisfying these conditions, the surfactant molecules are instinctively incorporated into different-shaped micelles, depending on the packing parameter (g), which is defined as, $g = v_0/(a_e l_0)$, where v_0 represents the hydrophobic tail volume of the surfactant, a_e represents the equilibrium area of the head group at the aggregate surface and l_0 represents the tail length.[100] Increasing the value of g results in the increased curvature of the interface

formed between the micelle and solution, and hence ends up in spherical, disc-like or rod-shaped micelles, and a value greater than 1 results in the formation of reverse micelles.[42,100] Thus, the packing parameter helps both in resolving the micelle shape and the packing shape. A representation of the various shaped micelles is presented in Fig. 4 and the relation between the packing parameter and micelle and packing shapes is given in Table 2. On being subject to the suitable chemical or electro-chemical reactions explained in the previous sections, these diverse-shaped micelles can be promptly used as soft-templates to guide the formation of the respectively-shaped nanostructures.[101]

Surfactant-assisted synthesis is among the oldest methods for the successful fabrication of TMOs. Numerous TMOs have been synthesized using diverse surfactants, and the last decade has witnessed great advancement in this area. Various types of ionic and non-ionic surfactants such as cetyl-trimethylammonium bromide (CTAB), polyvinylpyrrolidone (PVP), and Triton-X have been used for this synthesis strategy. Typical examples of TMOs with diverse morphologies synthesized with the aid of different surfactants are provided in Fig. 5. Among these surfactants, CTAB has attracted great interest owing to its exceptional structure guiding, agglomeration inhibiting and crosslinking properties, which stimulate it to regulate the microstructure formation and specific morphologies. Yayapao et al. synthesized orthorhombic WO_3 micro-flowers with a large number of petals using the CTAB-assisted hydrothermal method.[102] The attraction of the cationic CTAB
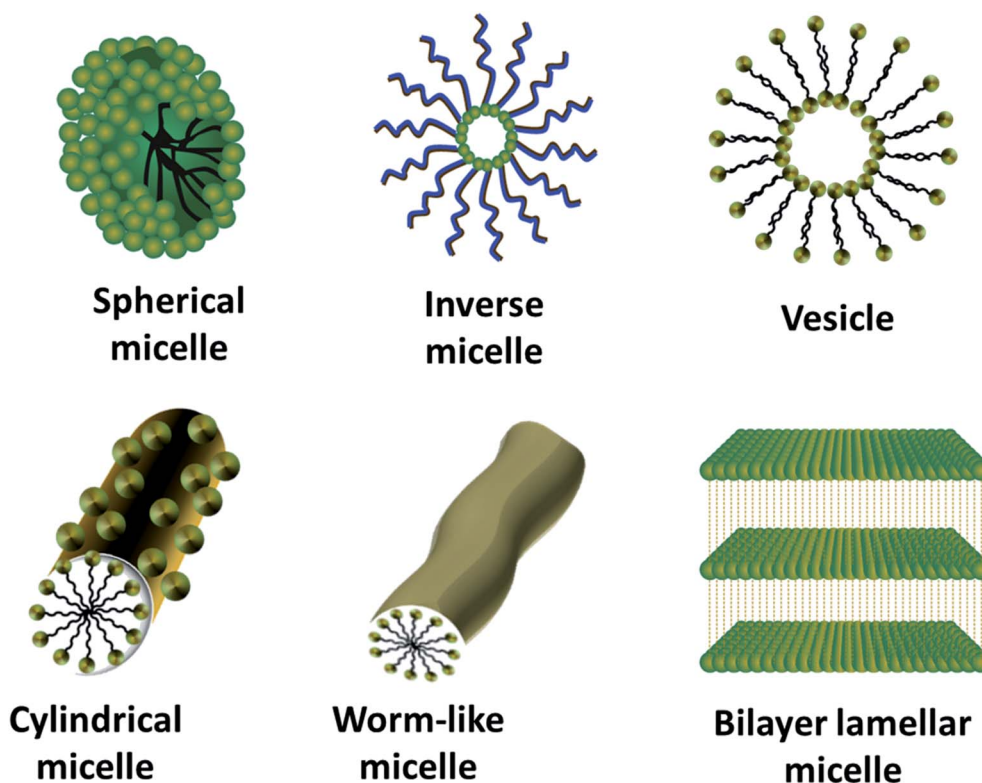

Fig. 4 Schematic representation of different-shaped micelles ranging from spherical micelles ($g \leq 1/3$) to bilayer lamellar micelles ($g = 1$).

Table 2   Relationship between the packing parameters and micelle shapes and packing shapes

g value	The extent of the curvature of the interface between micelle and solution	Micelle shape	Packing shape
$g \leq 1/3$	High	Spherical micelle	Cone
$1/3 < g \leq 1/2$	Medium	Elliptical micelle	Truncated cone
$1/2 < g \leq 1$	Low	Disc-like micelle	Truncated cone
$g = 1$	Very low	Bilayers	Cylindrical

towards the negatively charged oxygen of the intermediate product resulted in the growth of petals in the desired direction for the formation of WO_3 microflowers. Li et al. came out with three interesting morphologies for nanostructured VO_2 for application in lithium-ion batteries. The three diverse morphologies, nanobelts, nanoflowers and nanoflakes, were obtained by making slight modifications in the CTAB surfactant used, along with the precursors and reaction time.[103] The effect of CTAB on the morphology of ZnO was also studied recently by Amrithavalli et al., where different-shaped ZnO nanoparticles were synthesized by controlling the precursor : surfactant ratio.[104] The formation of ZnO nanoparticles was achieved by the interaction of the surfactant with the zincate oligomers formed in the course of the reaction and a change in morphology was observed from edge-rounded triangular to rough-edged quadrilateral with the increase in the precursor ratio. Thus, the introduction of the surfactant plays a major role in the morphology of the final products. It is also known that the concentration of the surfactant and the reaction conditions also regulates the shape of the micelles, which in turn acts as the predominant factor for the structure guiding properties of the surfactant.

Another important surfactant used for the fabrication of TMOs is PVP, which is categorized as a non-ionic surfactant. Wang et al. fabricated multi-shelled hollow spheres of Co_3O_4 as anode materials in lithium-ion batteries by PVP-assisted solvothermal method.[105] The optimal control of the concentration of PVP in the presence of cobalt glycolate resulted in the development of multilamellar PVP micelles with varying shell numbers, which caused the formation of multi-shelled hollow spheres on further annealing. Cao et al. utilized PVP for the synthesis of highly-ordered VO_2 hollow spheres.[106] PVP, in the initial stages, might serve as a shape controller or a ligand for the coordination of the precursor, but later forms spherical micelles for the adsorption of the precursor molecule. Under the control of the added PVP surfactant, the nanorods formed from the interconnected nanoparticles circle around to form the hollow microspheres. Cao et al. used the structure-directing properties of PVP for the preparation of polycrystalline belt-like ZnO nanowires.[107] Here, PVP serves as both a shape controller, by preventing the rapid growth of ZnO nanocrystallites into fractal morphologies, and as a controller of the ordered self-assembly of ZnO particles for the formation of ZnO belts. Triton-X and polyvinyl alcohol (PVA) are other important neutral surfactants employed for the synthesis of various TMOs. Dubal et al. synthesized MnO_2 thin-films by the surfactant-assisted electrodeposition method with the aid of Triton-X.[108]

The presence of the surfactant resulted in the formation of uniform thin-films of higher surface area with increased numbers of pores. The surfactant also promoted the retainment of the amorphous character of the film with superhydrophilic nature. These features have resulted in the strengthening of the core by preventing capacity loss, leading to greater capacitance. Dubal et al. also extended their work to the synthesis of CuO thin-films grown on stainless steel substrates.[109] The surfactant-assisted chemical bath deposition method was employed for the synthesis, where Triton-X was used as the surfactant and the physicochemical properties of the obtained CuO were compared with the CuO synthesized using another surfactant, PVA. Though the product formed via both the surfactants retained the crystallinity, there was much variation in the surface properties and activity. PVA, with the help of its –OH group, was adsorbed on the smaller grown particles, leading to the formation of flower-like nanostructures, whereas, in the case of Triton-X, the nanoscale segregation of the organic-rich area on the growing CuO particles led to the formation of 3D curved flower-like nanostructures. Thus, the surface area and porosity of Triton-X aided CuO is greater than that of the PVA-aided CuO, which resulted in the enhanced electrochemical activity of Triton-X-synthesized CuO.

Another category of anionic surfactant used for the fabrication of TMOs is sodium dodecyl sulfate (SDS). Several TMOs with distinct properties have been synthesized using SDS as the soft-template. For example, Zhang et al. synthesized CuO nanoparticles, which were attached to SDS-functionalized macroporous carbon.[110] The functionalization of macroporous carbon using the self-assembly of SDS resulted in the proper dissolution of macroporous carbon and the uniform and firm incorporation of CuO nanoparticles onto its surface by taking advantage of the electrostatic interactions between negatively charged SDS and Cu^{2+} ions. The surfactant-assisted synthesis of oxides of copper had also been studied by Lou et al., where Cu_2O crystals were obtained by the surfactant-assisted electrodeposition method.[111] Here, SDS acted as both a mediator for inhibiting the aggregation of the products and a shape regulator for the fabrication of polyhedral crystals. Apart from these, there are a number of surfactants such as polyethylene glycol (PEG), tetraoctylammonium bromide (TOAB) and tetrabutylammonium hydroxide (TBAOH), which are used for the synthesis of TMOs. Akram et al. came up with a low-temperature surfactant-assisted synthesis of sub-10 nm TiO_2 nanocrystals with excellent photocatalytic activity.[112] Here, polyethylene glycol (PEG) was used as the surfactant to restrict the agglomeration and facilitate the development of
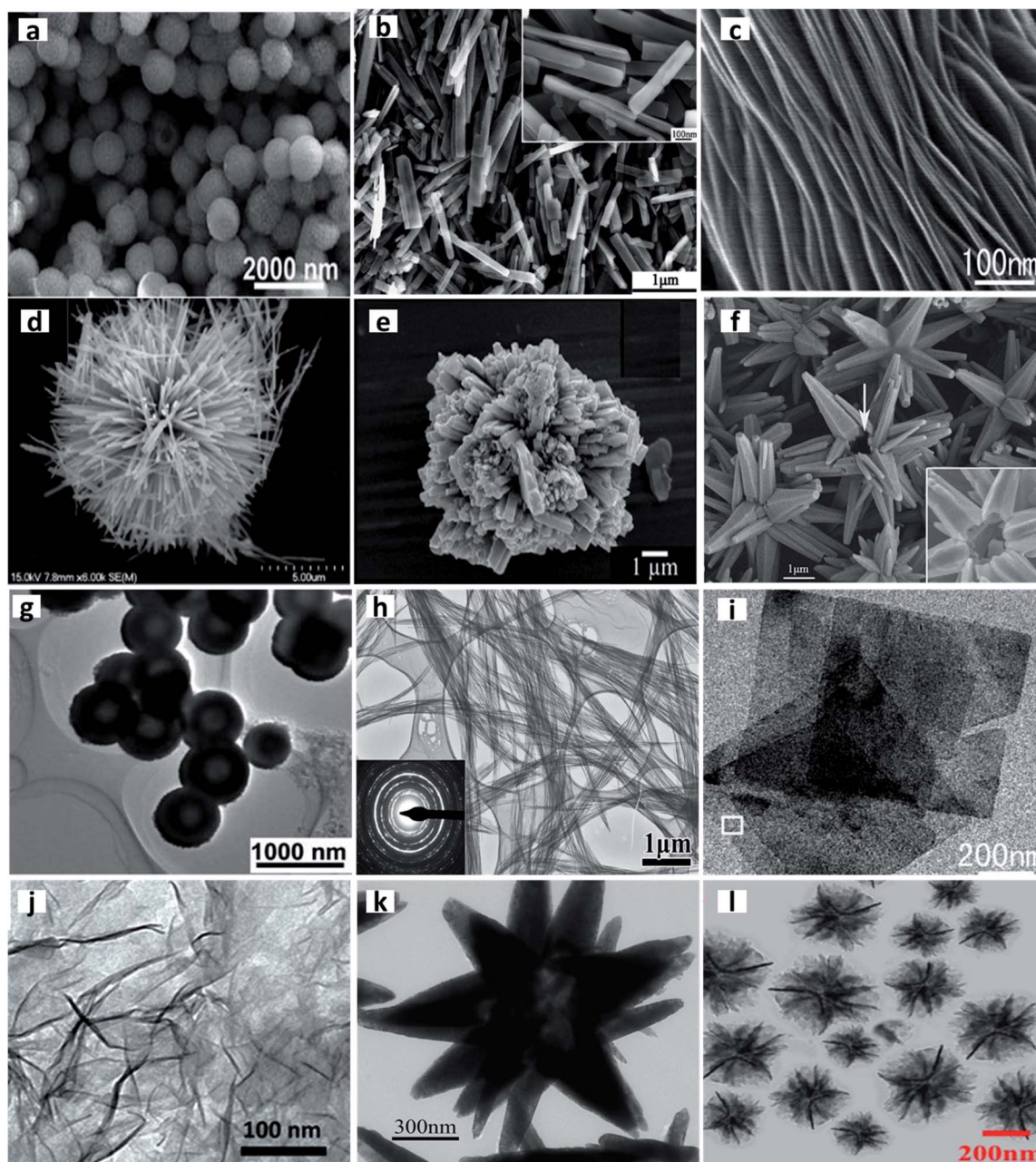
Fig. 5 Typical examples of TMOs with diverse morphologies synthesized with the aid of different surfactants. SEM images of (a) Cu_2O hollow spheres. Reproduced from ref. 159 with permission from The Royal Society of Chemistry. (b) $VO_2(B)$ nanobelts. Reprinted from Li N., Huang W., Shi Q., Zhang Y. and Song L., A CTAB-assisted hydrothermal synthesis of $VO_2(B)$ nanostructures for lithium-ion battery application, *Ceram. Int.*, 39, 6199–6206. Copyright (2013), with permission from Elsevier. (c) TiO_2 nanosheets. Reproduced from ref. 212 with permission from The Royal Society of Chemistry. (d) Urchin-like MnO_2, Reprinted with permission from ref. 183. Copyright (2007) American Chemical Society. (e) WO_3 microflowers. Reprinted from Yayapao O., Thongtem T., Phuruangrat A. and Thongtem S., CTAB-Assisted Hydrothermal Synthesis of Tungsten Oxide Microflowers, *J. Alloys Compd.*, 509, 2294–2299, Copyright (2010), with permission from Elsevier. (f) Multigonal star-shaped ZnO. Reprinted from Hu H., Deng C. and Huang X., Hydrothermal Growth of Center-Hollow Multigonal Star-Shaped ZnO Architectures Assembled by Hexagonal Conic Nanotubes, *Mater. Chem. Phys.*, 121, 364–369, Copyright (2010), with permission from Elsevier. TEM images of (g) Cu_2O hollow spheres. Reproduced from ref. 159 with permission from The Royal Society of Chemistry. (h) CuO nanowire bundle. Reprinted from Li Y., Yang X. Y., Rooke J., Tendeloo G. Van and Su B. L., Ultralong $Cu(OH)_2$ and CuO Nanowire Bundles: PEG200-Directed Crystal Growth for Enhanced Photocatalytic Performance, *J. Colloid Interface Sci.*, 348, 303–312, Copyright (2010), with permission from Elsevier. (i) TiO_2 nanosheet. Reproduced from ref. 212 with permission from The Royal Society of Chemistry, (j) MnO_2 nanosheet. Reproduced with permission under a Creative Commons CC-BY License from Liu Z., Xu K., Sun H. and Yin S, One-Step Synthesis of Single-Layer MnO_2 Nanosheets with Multi-Role Sodium Dodecyl Sulfate for High-Performance Pseudocapacitors, *Small*, 2015, 11, 2182–2191. Copyright 2015 John Wiley and Sons. (k) ZnO hollow star. Reprinted from Hu H., Deng C. and Huang X., Hydrothermal Growth of Center-Hollow Multigonal Star-Shaped ZnO Architectures Assembled by Hexagonal Conic Nanotubes, *Mater. Chem. Phys.*, 121, 364–369, Copyright (2010), with permission from Elsevier. (l) Cu_2O nanoflowers. Reprinted from Cao S., Chen H., Han T., Zhao C. and Peng L., Rose-like Cu_2O Nanoflowers *via* Hydrothermal Synthesis and Their Gas Sensing Properties, *Mater. Lett.*, 180, 135–139, Copyright (2016), with permission from Elsevier.

smaller-sized nanocrystals. The concentration of the surfactant was found to have a pronounced effect on the particle size. Zhang *et al.* synthesized mesoporous ribbon-like CuO using TOAB as the surfactant.[113] Here, the growth pattern was controlled by the preferential binding of the positive head group of TOAB to the negatively charged precursor surface. Leng *et al.* introduced a novel exfoliation method for the synthesis of single-layer TiO_2 nanosheets with the aid of a surfactant TBAOH.[114] Here, the surfactant played a major role in retaining the 2D structure and developing the bulk quantity of nanosheets with increased capacitance by preventing the rolling up of the nanosheets formed to develop nanotubes. In certain cases, a mixture of surfactants is employed for the synthesis of TMOs with desired properties. For instance, Zhang *et al.* utilized a mixture of CTAB and PVP to control the shape and size of octahedral Mn_3O_4 crystallites.[115] The adoption of the CTAB/PVP mixture resulted in the formation of well-ordered octahedral nanocrystals, whereas, the reaction in the presence of a single surfactant resulted in large-scale agglomeration.

It is, therefore, evident that the surfactant plays a crucial role in controlling the nanostructures as shown in the consolidated morphologies of TMOs (Fig. 6). Since the use of different surfactants may result in the formation of the same material with diverse properties, the judicious choice of surfactant is a crucial step in the synthesis of TMOs.

4.3 Synthesis of TMOs with block copolymers as a soft-template

Block copolymers refer to high polymers composed of two or more chemically discrete polymer chains combined at the ends by covalent bonds and can be self-assembled to a wide variety of ordered structures. By virtue of the presence of different blocks with diverse properties, block copolymers can be easily molded into different morphologies, from thin-films to 3D templates, for the synthesis of varied structured TMOs.[50] As shown in Fig. 7, the general synthesis strategy for the block copolymer-assisted synthesis includes (1) the micelle formation of the copolymers, (2) precursor addition, and (3) self-assembly to a definite shape. The removal of the template thus results in the formation of the final product with the desired morphology. There are certain synthesis conditions to be followed for the successful synthesis of the products *via* copolymer-assisted synthesis, including a strong interaction between the precursor molecule and any of the blocks of the copolymer, the effective cross-linking of the precursor with higher thermal stability than that of the template, and the successful formation of the micelle by the copolymer.[116] Based on the intermolecular interactions stimulating the segregation of the core part, block copolymer micelles may be grouped into amphiphilic micelles, polyion complex micelles and micelles formed from metal complexation.[117] The shape of the formed micelle depends on the relative length of the hydrophilic segment, a longer hydrophilic segment results in spherical micelles and a longer core segment results in non-spherical structures like lamellae or rods.[117]

The fabrication of TMOs using block copolymers as a soft-template has been explored for decades. The first work on the synthesis of TMOs by using block copolymers was introduced by Yang *et al.* in 1998,[118] and was extended to a deeper level in 1999.[119] He introduced a simple method for the synthesis of a large number of TMOs and mixed TMOs including ZrO_2, TiO_2, Nb_2O_5, WO_3, Ta_2O_5, $ZrTiO_y$, ZrW_2O_y by using amphiphilic poly(alkylene oxide) as the block copolymer template and inorganic salts as the precursor. Here, the formation of mesoporous TMOs proceeded *via* complexation of the inorganic precursor with the self-assembled block copolymer. The TMOs thus formed were thermally stable and possessed strong inorganic frameworks for the nucleation of highly dense nanocrystallites. Even after a decade of this exploration, the facile synthesis of the thermally stable TMOs still posed a challenge. Lee *et al.*, in 2008, reported the synthesis of crystalline mesoporous TMOs, TiO_2 and Nb_2O_5 using diblock copolymers.[120] Here, a combined soft and hard approach (CASH) was employed by incorporating the block copolymer, poly(isoprene-*block*-ethylene oxide) with sols of TMOs. Later, Brezesinski *et al.* synthesized highly ordered mesoporous α-MoO_3 for pseudosupercapacitor applications.[121] Here, highly crystalline TMOs were formed using poly(ethylene-*co*-butylene)-*b*-poly(ethylene oxide) block copolymer. These highly crystalline TMOs with van der Waals gaps and interconnected mesoporosity were used as excellent pseudocapacitors. Tanaka *et al.* fabricated mesoporous iron oxide using poly(styrene-*b*-acrylic acid-*b*-ethylene glycol) (PS-*b*-PAA-*b*-PEG) triblock copolymer for the detection of glucose.[122] Each block in the copolymer system has its specific functionalities. The PS block, owing to its lower solubility in water, constituted the core of the micelle, the carboxylate ions of the anionic PAA block linked with the cationic metal ion forming the shell and the hydrophilic PEG block constituted the corona of the micelle, which inhibited the secondary aggregation. Bastakoti *et al.* presented the polymeric micelle assembly for the synthesis of mesoporous TMOs such as TiO_2, Ta_2O_5, Nb_2O_5 using a triblock copolymer poly(styrene-*b*-2-vinyl pyridine-*b*-ethylene oxide) (PS-*b*-PVP-*b*-PEO).[86] The hydrophobic PS block stabilized the spherical micelles and acted as a template for the fabrication of TMOs with larger pores. The cationic PVP unit functioned as coordinating ligands for promoting the interaction with inorganic precursors for the fabrication of highly stronger walls, and the good dispersion of the micelles in the precursor solution was ensured by the hydrophilic PEO corona, resulting in the ordered packing of the micelles. Zhu *et al.* employed the ligand-aided solvent evaporation stimulated co-assembly technique for the preparation of ordered mesoporous WO_3 for the detection of pathogens.[123] Here, the tailor-made diblock copolymer poly(ethylene oxide)-*b*-polystyrene (PEO-*b*-PS) was used as the soft-template for the synthesis. The alteration of the length of the hydrophobic PS segment in the diblock resulted in tuning the pore size of crystalline WO_3 for the desired application. The chelation-aided soft-templating technique is yet another synthesis strategy for the preparation of TMOs. Zhou *et al.* employed this method for the synthesis of ordered mesoporous ZnO by using diblock copolymer poly(ethylene oxide)-*b*-polystyrene (PEO-*b*-PS) as the soft-template and citric acid as the
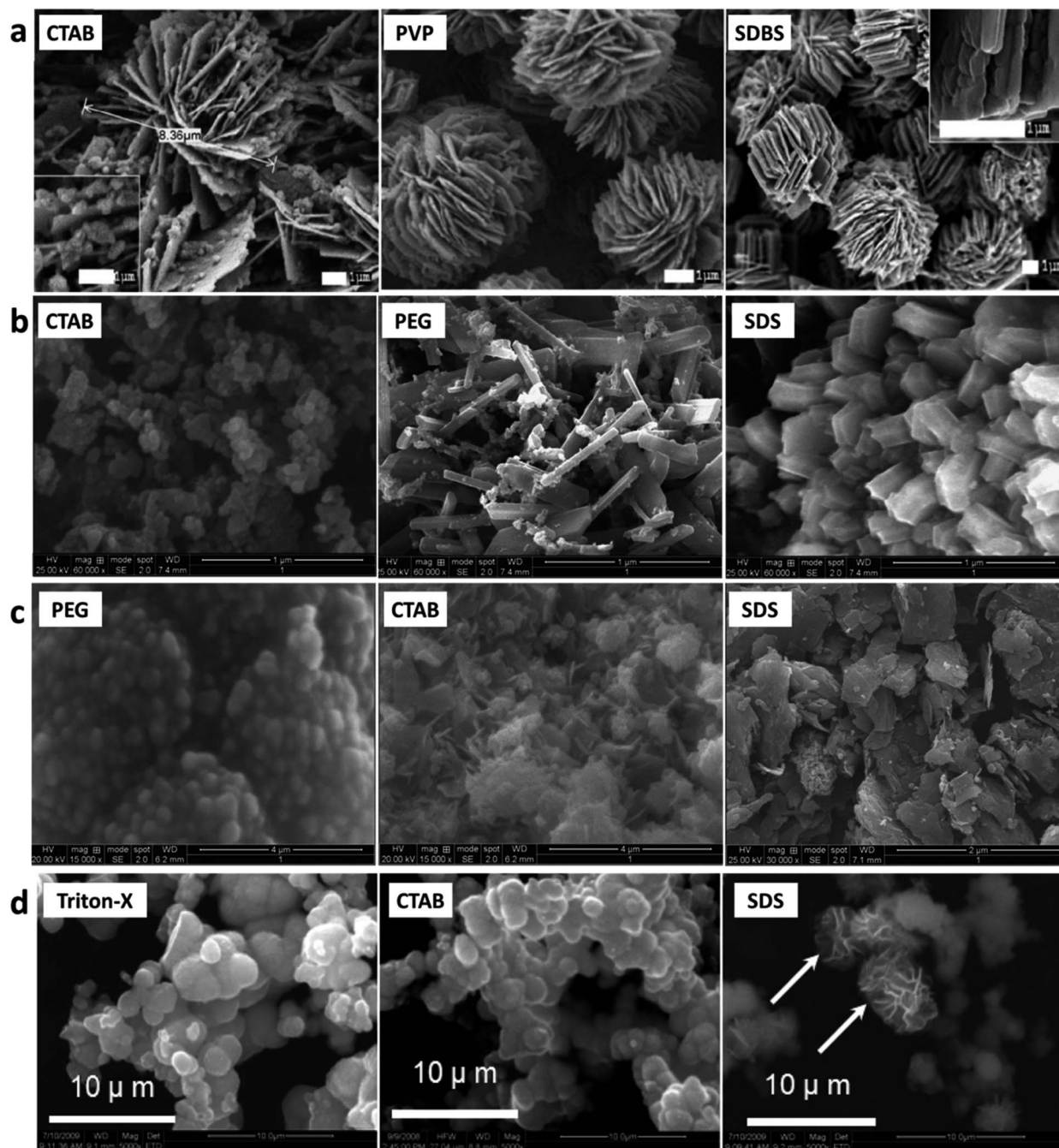
Fig. 6 Diverse morphologies of the same TMOs synthesized using different surfactants. (a) V_2O_5. Reprinted from Hu B., Cheng H., Huang C., Aslam M. K., Liu L., Xu C., Chen P., Yu D. and Chen C., The Controlled Study of Surfactants on the Morphologies of Three-Dimensional Turbine-like V_2O_5 for the Application of High-Performance Lithium-Ion Storage, *Solid State Ionics*, **342**, 115059, Copyright (2019), with permission from Elsevier. (b) NiO. Reprinted from Rajendran V. and Anandan K., Different Ionic Surfactants Assisted Solvothermal Synthesis of Zero-, Three and One-Dimensional Nickel Oxide Nanostructures and Their Optical Properties, 203–208, *Mater. Sci. Semicond. Process.*, **38**, Copyright (2015), with permission from Elsevier. (c) Cr_2O_3. Reprinted from Anandan K. and Rajendran V., Sheet, Spherical and Plate-like Chromium Sesquioxide (Cr_2O_3) Nanostructures Synthesized *via* Ionic Surfactants-Assisted Facile Precipitation Method, *Mater. Lett.*, **146**, 99–102, Copyright (2015), with permission from Elsevier. (d) NiO. "Reprinted with permission from ref. 197. Copyright (2010) American Chemical Society."

chelating agent.[124] The decomposition of the soft-template and the intermediate resulted in the formation of the highly ordered crystalline ZnO with desired pores for the sensing application of ethanol. The peculiar morphologies of TMOs synthesized *via* various block copolymer-assisted methods are demonstrated in Fig. 8.

4.4 Synthesis of TMOs with biological soft-templates

The use of biological substances as soft-templates is an incredible concept and various research efforts have been conducted in this area to utilize the readily available and inexpensive biological materials for the fabrication of TMOs with

Fig. 7 Schematic diagram of the general synthesis strategy of the block copolymer–assisted synthesis of TMOs.

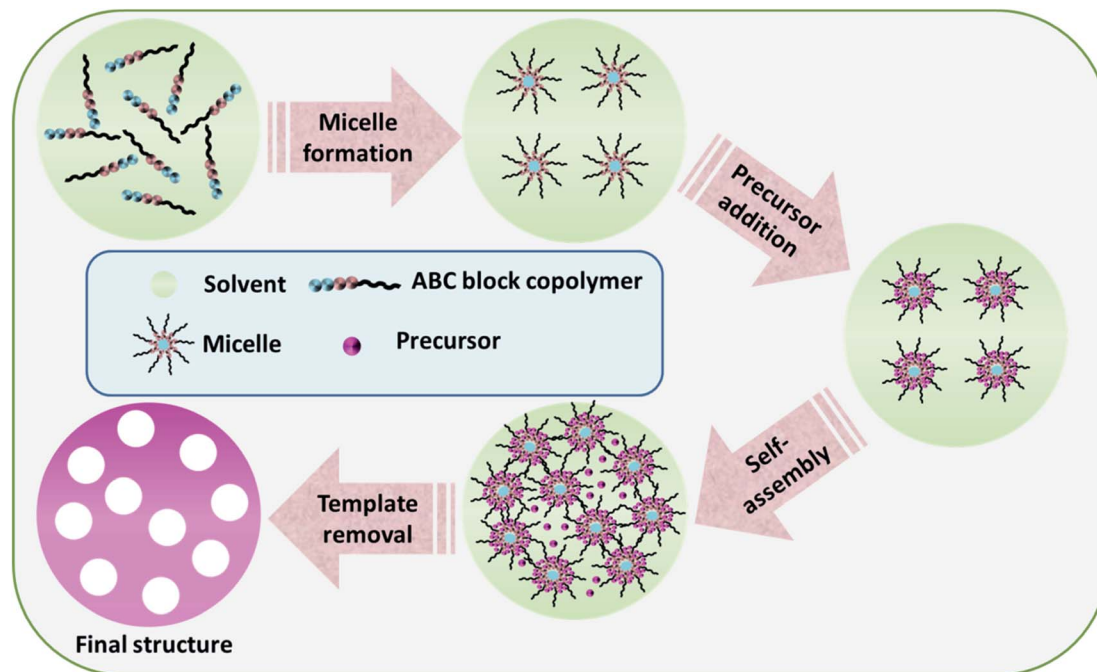controlled properties. Different categories of biological materials, including biomolecules, unicellular organisms, and complex tissues can be used as soft-templates (Fig. 9).[42] The naturally existing unique structure of this biological template outweighs the synthetically made templates, and facilitates exceptional chemistry on the template, promoting the formation of TMOs with controlled morphology, composition and crystal structure.[50] Biomolecules and their naturally existing clusters like peptides, proteins and DNA can serve as soft-templates for the synthesis of TMOs. Peptides or protein template synthesis, owing to its simplicity, better biocompatibility and high control over the crystallinity have been widely employed for the fabrication of TMOs. Kim *et al.* came out with a rational synthesis technique for the synthesis of WO$_3$ nanofibres functionalized with nanoparticles by using a polar protein nanocage as the template.[125] The protein nanocage consisted of a hollow apoferritin for enclosing the nanoparticles whose bulk agglomeration was hindered by the protein template. The further decomposition of the protein shell resulted in the formation of WO$_3$ microstructures with desired pores for the detection of trace amounts of biomarkers in the exhaled breath. Kashyap *et al.* visualized the nucleation process of iron oxide nanoparticles facilitated by an acidic bacterial recombinant protein, Mms6.[126] The protein self-assembly and the micellar iron-binding inhibited the nucleation outside the micelles and the aggregation during the nucleation, thus providing an easy pathway for further nucleation by lowering the energy barrier. Han *et al.* employed bovine-serum albumin (BSA) as the protein-template for the fabrication of 2D MnO$_2$ nanoflakes for the colorimetric detection of glucose.[127] Since MnO$_2$ nanoflakes exhibit dual enzyme activity, a one-pot

strategy for the detection of glucose without the aid of enzymes was also introduced.

DNA molecules have also been distinguished for their ability to act as templates for nanostructure fabrication. As a reference, Hassanien *et al.* employed DNA strands as the templates for the self-assembly of conductive Cu$_2$O nanowires without the requirement of complex techniques.[128] Here, Cu$_2$O nanostructures were assembled on λ-DNA by undergoing a chemical reduction in the presence of Benedict's reagent and ascorbic acid. The transformation of Cu$_2$O from nanoparticles to nanowires was studied by means of atomic force microscopy, and it was observed that the Cu$_2$O nanoparticles attached initially to λ-DNA formed a beads-on-a-string morphology, which gradually transformed into smooth nanowires with time. Ede *et al.* developed a new approach for the evolution of different-shaped β-MnO$_2$ on a DNA scaffold for catalytic and supercapacitor applications.[129] Here, two diverse morphologies, wire-like and flake-like, were obtained by adjusting the DNA : precursor molar ratio along with the reaction conditions in the aqueous phase synthesis. The reaction advanced *via* the adsorption of the Mn^{2+} ions on the negatively charged phosphate group of DNA to form the Mn^{2+}-DNA complex, which later got converted into MnO$_2$ in the presence of NaOH and atmospheric oxygen. The lower concentration of DNA facilitated the MnO$_2$ particles growing into helical DNA structures, resulting in wire-like MnO$_2$, whereas a higher concentration of DNA facilitated the aggregation of MnO$_2$ particles into flake-like structures.

Other important categories of biological templates include bacterial, viral, and fungal templating. These are certainly promising techniques for the large-scale formation of different micro/nanostructures. One of the typical bacteria used as biotemplates is *Bacillus subtilis*, which is a Gram-positive species.
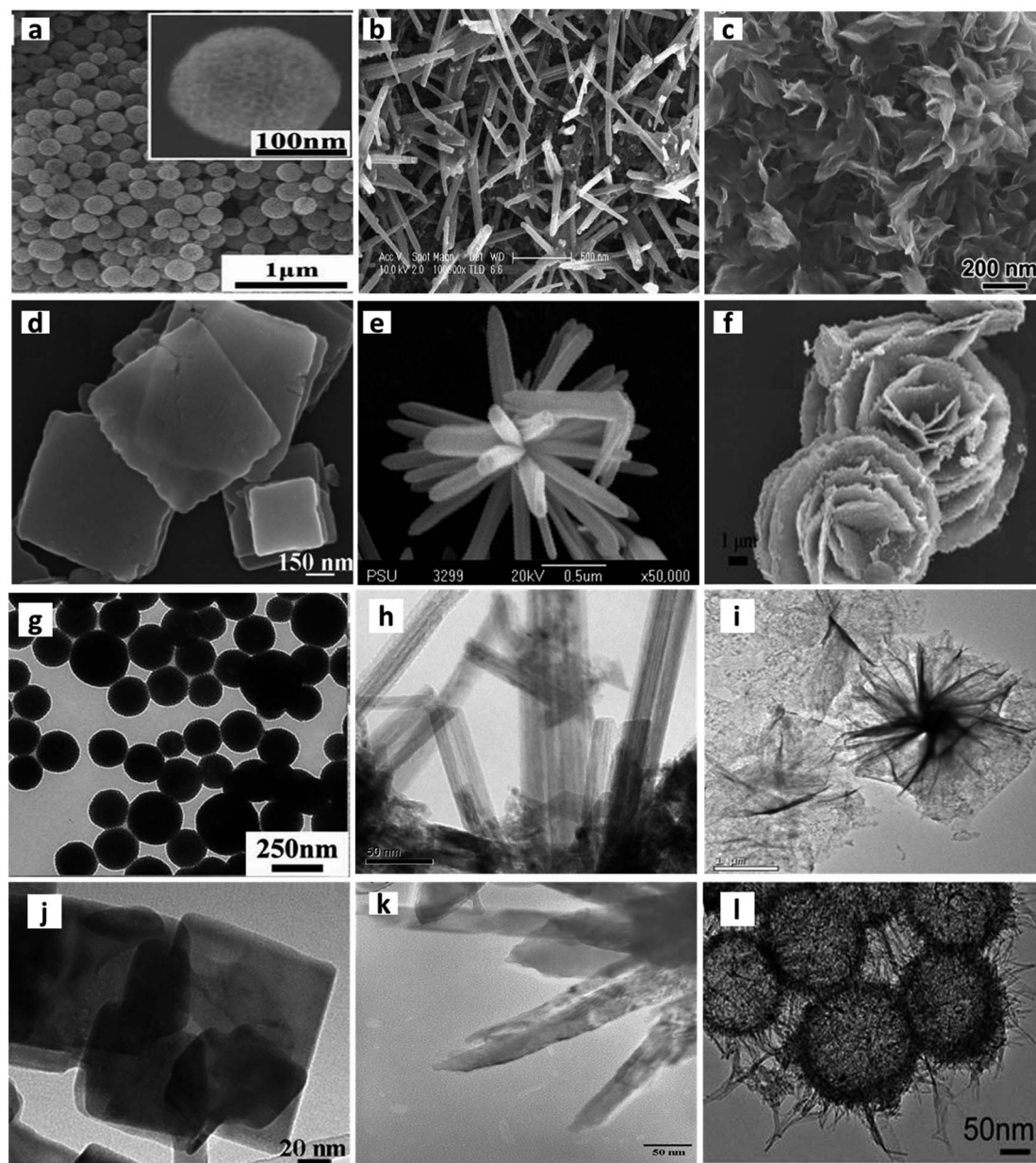
Fig. 8 Typical examples of TMOs with diverse morphologies synthesized with the aid of different block copolymers. SEM images of (a) Cu_2O mesoporous spheres. Reproduced from ref. 252 with permission from The Royal Society of Chemistry. (b) MnO_2 nanorods. Reprinted from Nayak P. K. and Munichandraiah N., Rapid Sonochemical Synthesis of Mesoporous MnO_2 for Supercapacitor Applications, *Mater. Sci. Eng., B*, **177**, 849–854, Copyright (2012), with permission from Elsevier. (c) TiO_2 nanosheets. Reprinted from Sheng L., Liao T., Kou L. and Sun Z., Single-Crystalline Ultrathin 2D TiO_2 Nanosheets: A Bridge towards Superior Photovoltaic Devices, *Mater. Today Energy*, **3**, 32–39, Copyright (2017), with permission from Elsevier. (d) WO_3 nanosheet. Reprinted from Wang Z., Wang D. and Sun J., Controlled Synthesis of Defect-Rich Ultrathin Two-Dimensional WO_3 Nanosheets for NO_2 Gas Detection, *Sens. Actuators, B*, **245**, 828–834, Copyright (2017), with permission from Elsevier. (e) Spherical ZnO nanorods. Reproduced from Amornpi-toksuk P., Suwanboon S., Sangkanu S., Sukhoom A. and Muensit N., Morphology, Photocatalytic and Antibacterial Activities of Radial Spherical ZnO Nanorods Controlled with a Diblock Copolymer, *Superlattices Microstruct.*, **51**, 103–113, Copyright (2012), with permission from Elsevier. (f) Fe_3O_4 nanoroses. "Reprinted with permission from ref. 262. Copyright (2010) American Chemical Society." TEM images of (g) Cu_2O mesoporous spheres. Reproduced from ref. 252 with permission from The Royal Society of Chemistry. (h) MnO_2 nanorods. Reprinted from Nayak P. K. and Munichandraiah N., Rapid Sonochemical Synthesis of Mesoporous MnO_2 for Supercapacitor Applications, *Mater. Sci. Eng., B*, **177**, 849–854, Copyright (2012), with permission from Elsevier. (i) Co_3O_4 nanosheet. Reprinted from Yang J., Gao M., Lei J., Jin X., Yu L. and Ren F., Surfactant-Assisted Synthesis of Ultrathin Two-Dimensional Co_3O_4 Nanosheets for Applications in Lithium-Ion Batteries and Ultraviolet Photodetector, *J. Solid State Chem.*, **274**, 124–133, Copyright (2019), with permission from Elsevier. (j) WO_3 nanosheet. Reprinted from Wang Z., Wang D. and Sun J., Controlled Synthesis of Defect-Rich Ultrathin Two-Dimensional WO_3 Nanosheets for NO_2 Gas Detection, *Sens. Actuators, B*, **245**, 828–834, Copyright (2017), with permission from Elsevier. (k) Spherical ZnO nanorods. Reproduced from Amornpitoksuk P., Suwanboon S., Sangkanu S., Sukhoom A. and Muensit N., Morphology, Photocatalytic and Antibacterial Activities of Radial Spherical ZnO Nanorods Controlled with a Diblock Copolymer, *Superlattices Microstruct.*, **51**, 103–113, Copyright (2012), with permission from Elsevier. (l) Urchin-like MnO_2 hollow nanosphere. Reproduced from ref. 268 with permission from the Centre National de la Recherche Scientifique (CNRS) and The Royal Society of Chemistry.
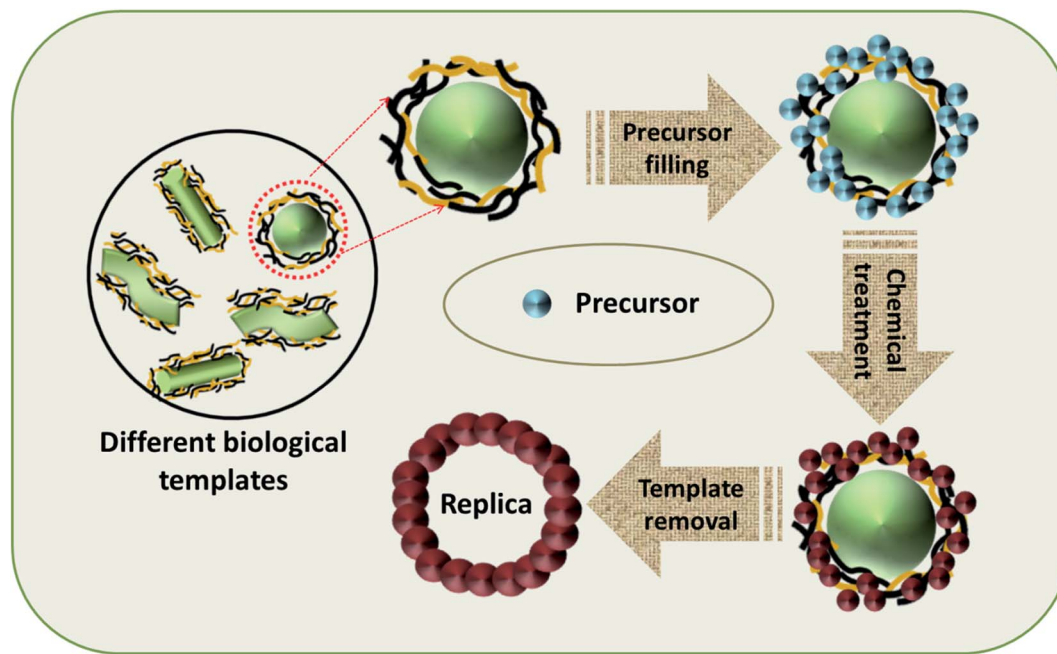
Fig. 9 Schematic representation of the biological template–assisted synthesis of TMOs.

Shim *et al.* used this bacteria as a template for the fabrication of rod-type porous Co_3O_4 with enhanced surface area and electrochemical activity.[130] The electrostatic synergy between the functional surfaces of the bacteria and the cobalt ions was used for the uniform crystallization of Co_3O_4 on the surface of the bacterial template. They further applied this strategy using the same bacteria for the synthesis of rod- and hollow-shaped manganese oxide.[131] Their group also reported 3D flower-like porous Co_3O_4 using another Gram-positive bacteria, *Micrococcus lylae*.[132] Chen *et al.* employed bacterial cellulose as a template for the polyol synthesis of ZnO nanoparticles with enhanced mechanical properties and photocatalytic activity.[133] The template served as both a matrix for the quantitative inclusion of Zn^{2+} ions and as a nanoreactor for the formation of ZnO nanoparticles. Zhou *et al.* introduced the facile synthesis of hollow TiO_2 with lactobacillus bacteria as a template.[134] The use of two different species of lactobacillus resulted in the generation of diverse hollow-sphere and tube-like TiO_2. The use of a virus as a soft-template for the synthesis of TMOs has also been a widely explored research area and various studies have been conducted in this field in the past decade. One of the most important viruses among them is the tobacco mosaic virus (TMV), which is a plant virus possessing a unique cylindrical shape with a high aspect ratio. Chu *et al.* adopted the TMV virus for the fabrication of hierarchical Ni/NiO electrodes with exceptional charge capacity.[135] The synthesis was facilitated by the thermal oxidation of electroless Ni-coated TMV, followed by a simple annealing technique. The role of TMV in the synthesis of ZnO nanostructures was studied by Atanasova *et al.*, where self-assembled TMV was used for the controlled synthesis of uniform ZnO nanowires as field-effect transistors.[136] TMV functioned both as a template for structure direction and as a facilitator for the

electron injection, resulting in the tuning of the properties of the semiconducting layer of the transistor. Another significant group of viruses used as bio-templates is M13, with excellent genetic tenability and replicability. Han *et al.* used genetically engineered M13 phages for the synthesis of MnO_2 nanowires for electrochemical sensing applications.[137] The nucleation and successive growth of MnO_2 crystals into nanowires was regulated by the surface charge of M13 mutants. The negatively charged M13 phages ended in the uniform distribution of MnO_2 crystals on the surface of the phage resulting in the formation of nanowires, whereas the weakly negative and positively charged phages ended in the irregular agglomeration of MnO_2. Virus-templated synthesis was also used for the synthesis of mixed TMOs. Oh *et al.* came out with the M13-assisted synthesis of mixed TMOs, cobalt manganese oxide nanowires for lithium–oxygen batteries.[138] With the aid of the M13 template, three diverse compositions of cobalt manganese oxide were prepared with diverse morphologies. The cobalt dominated systems exhibited a particle shape growth and the manganese dominated systems exhibited a planar shape growth. Though less reported, fungus-templated synthesis has also been employed for the preparation of TMOs. As a reference, He *et al.* synthesized hollow Cu_2O microspheres by using yeast as a bio-template.[139] The reaction proceeded *via* the formation of yeast/Cu^{2+} core–shell spheres by the coulombic interactions between negatively charged functional groups of the template and positively charged ions in the precursor. The yeast/Cu^{2+} core–shell spheres subsequently formed Cu_2O spheres on the addition of OH^- and glucose solution. Some of the explicit examples for the attainment of specific morphology with the aid of biological templates are presented in Fig. 10.
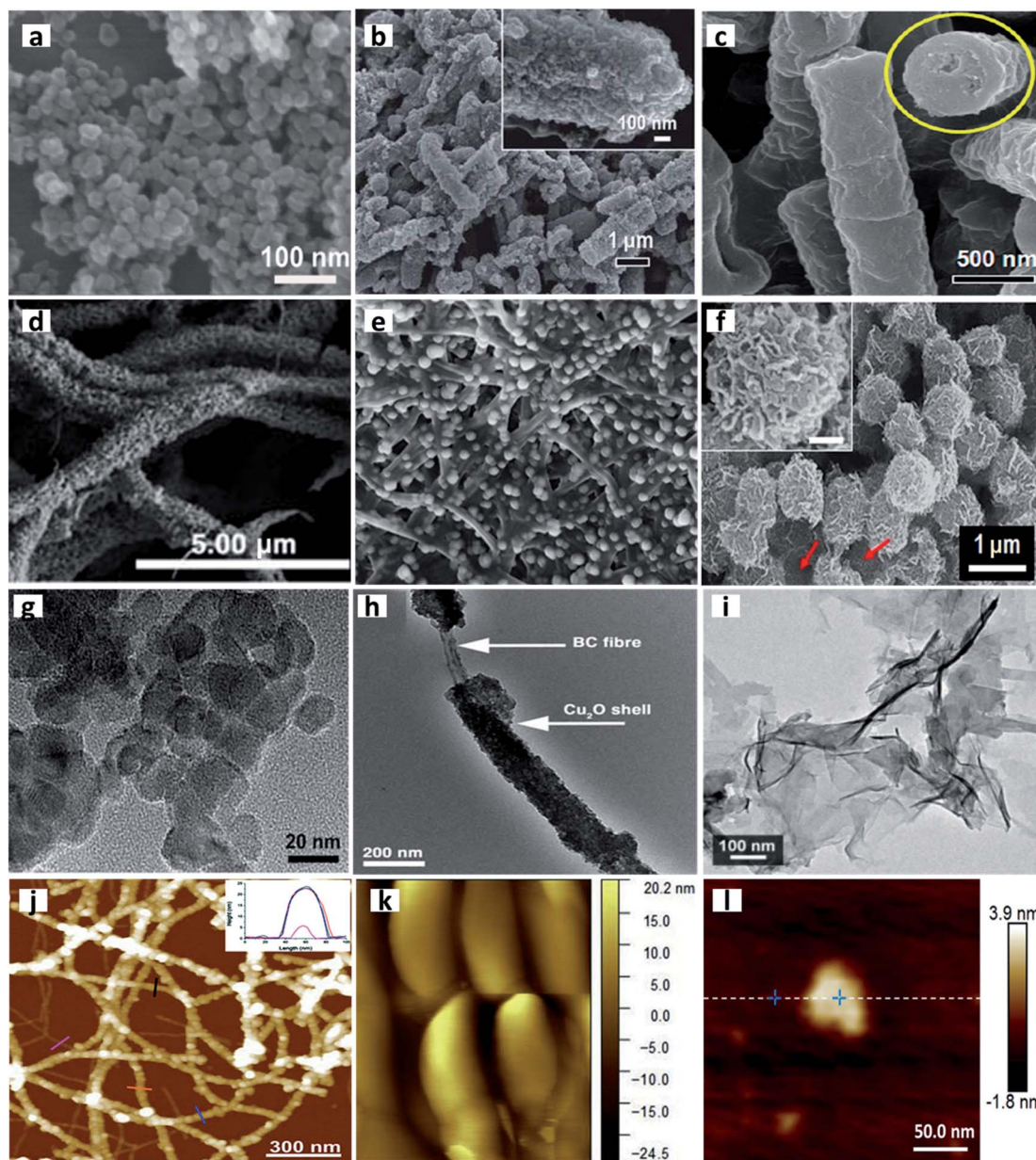
Fig. 10 Typical examples of TMOs with diverse morphologies synthesized with the aid of different biological templates. SEM images of (a) TiO$_2$ nanoparticles. Reprinted from Yu C., Li X., Liu Z., Yang X., Huang Y., Lin J., Zhang J. and Tang C., Synthesis of Hierarchically Porous TiO$_2$ Nanomaterials Using Alginate as Soft Templates, *Mater. Res. Bull.*, **83**, 609–614, Copyright (2016), with permission from Elsevier. (b) Bacteria/manganese oxide composite rods. Reproduced from ref. 131 with permission from The Royal Society of Chemistry. (c) Close-ended hollow Co$_3$O$_4$ rods. "Reprinted with permission from ref. 130. Copyright (2011) American Chemical Society." (d) Cu$_2$O microtubes. Reproduced from ref. 296 with permission from The Royal Society of Chemistry. (e) ZnO nanoparticles. Reprinted from Chen S., Zhou B., Hu W., Zhang W., Yin N. and Wang H., Polyol Mediated Synthesis of ZnO Nanoparticles Templated by Bacterial Cellulose, *Carbohydr. Polym.*, **92**, 1953–1959, Copyright (2013), with permission from Elsevier. (f) Flower-like Co$_3$O$_4$. Reproduced with permission from ref. 132. Copyright 2013 Springer Nature Publishing. TEM images of (g) TiO$_2$ nanoparticles. Reprinted from Yu C., Li X., Liu Z., Yang X., Huang Y., Lin J., Zhang J. and Tang C., Synthesis of Hierarchically Porous TiO$_2$ Nanomaterials Using Alginate as Soft Templates, *Mater. Res. Bull.*, **83**, 609–614, Copyright (2016), with permission from Elsevier. (h) Cu$_2$O microtubes. Reproduced from ref. 296 with permission from The Royal Society of Chemistry. (i) MnO$_2$ nanoflakes. Reproduced with permission under a Creative Commons CC-BY License from Han L., Zhang H., Chen D. and Li F., Protein-Directed Metal Oxide Nanoflakes with Tandem Enzyme-Like Characteristics: Colorimetric Glucose Sensing Based on One-Pot Enzyme-Free Cascade Catalysis, *Adv. Funct. Mater.*, 2018, **28**(17), 1–9. Copyright 2018 John Wiley and Sons. AFM images of (j) TiO$_2$ decorating the surface of amyloid fibrils. Reproduced with permission under a Creative Commons CC-BY License from Bolisetty S., Adamcik J., Heier J. and Mezzenga R., Amyloid Directed Synthesis of Titanium Dioxide Nanowires and Their Applications in Hybrid Photovoltaic Devices, *Adv. Funct. Mater.*, 2012, **22**(16), 3424–3428. Copyright 2012 John Wiley and Sons. (k) 2D ZnWO$_4$. Reprinted from Yesuraj J. and Suthanthiraraj S. A., Bio-Molecule Templated Hydrothermal Synthesis of ZnWO$_4$ Nanomaterial for High-Performance Supercapacitor Electrode Application, *J. Mol. Struct.*, **1181**, 131–141. Copyright (2019), with permission from Elsevier. (l) MnO$_2$ nanoflakes. Adapted with permission under a Creative Commons CC-BY License from Han L., Zhang H., Chen D. and Li F., Protein-Directed Metal Oxide Nanoflakes with Tandem Enzyme-Like Characteristics: Colorimetric Glucose Sensing Based on One-Pot Enzyme-Free Cascade Catalysis, *Adv. Funct. Mater.*, 2018, **28**(17), 1–9. Copyright 2018 John Wiley and Sons.
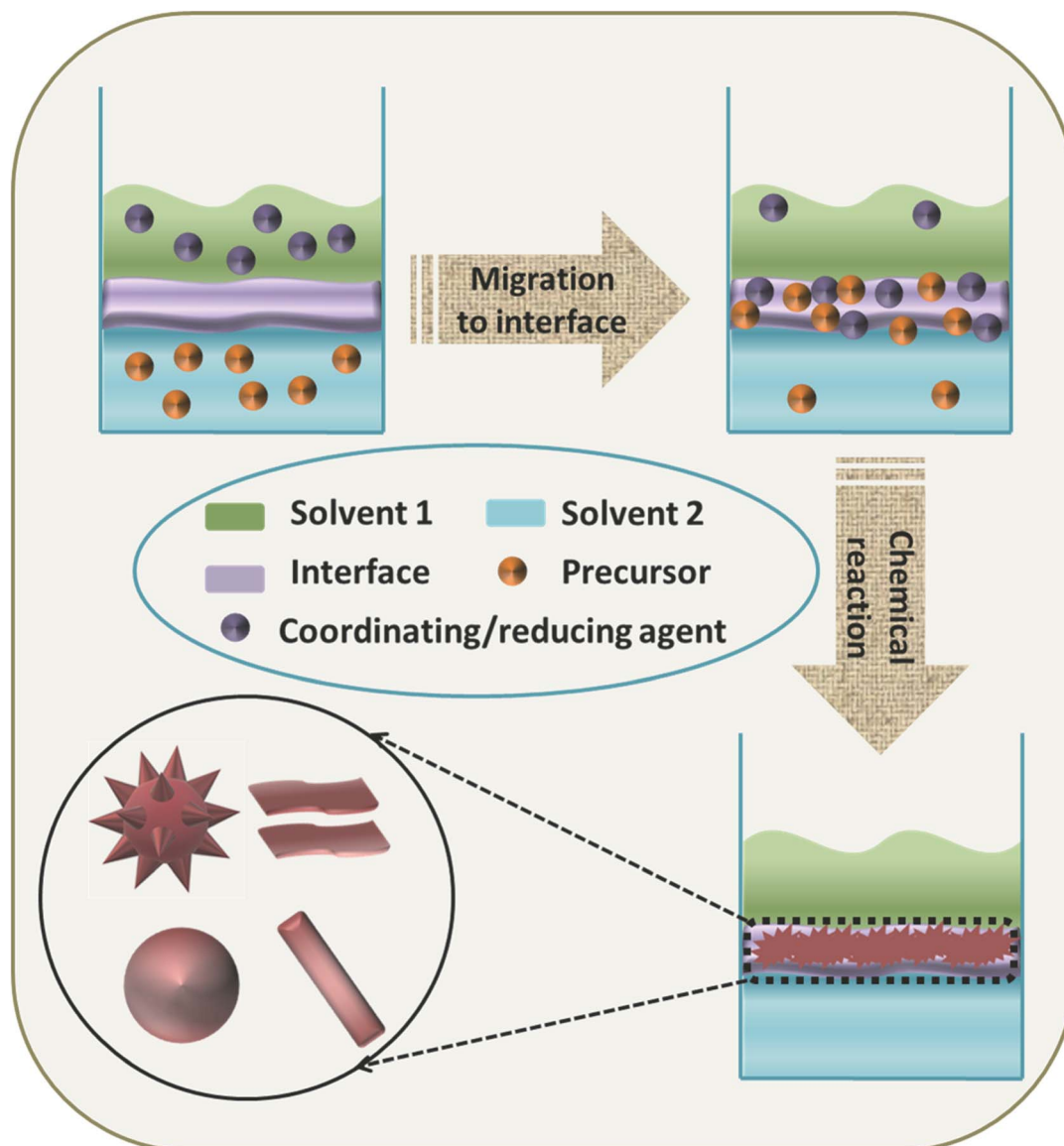
Fig. 11 Schematic diagram of the liquid/liquid interface-assisted synthesis of 0D, 1D, 2D or 3D TMOs.

4.5 Synthesis of TMOs with interfaces as the soft-template

Interface-assisted synthesis is an emerging versatile approach for the controlled synthesis of nanostructures with tuned morphologies. Interfaces adopted in chemical reactions include air/liquid, air/solid, liquid/liquid and liquid/solid, of which the liquid/liquid interface-assisted synthesis predominates in the fabrication of TMOs.[140] The interface is acclaimed to afford a unique non-equilibrium environment with enhanced surface energy for the assembly of precursors to initiate the nucleation, leading to further growth of the intermediates to form the final structure with desired morphology (Fig. 11).[140] The simple synthesis procedure without the requirement of the removal of the template along with the retainment of high crystallinity has driven the liquid/liquid interface-assisted synthesis to be a major technique for the fabrication of TMOs.

Though there are fewer reports on the interface-assisted synthesis of TMOs, the last few decades have observed advancements in this area of synthesis. Wang *et al.* made use of the water/air interface for the fabrication of nanometer-thick large-area and single-crystalline ZnO nanosheets.[141] The growth of nanosheets was facilitated by the epitaxial growth directed by the surfactant monolayer at the water/air interface. Among several interfaces, the liquid/liquid interface has been widely exploited for the synthesis of TMOs. The diverse morphologies of TMOs synthesized using the liquid/liquid interface as the soft-template are given in Fig. 12. Cheng *et al.* employed a benzene/water interface-aided solvothermal reaction for the synthesis of durian-like α-Fe$_2$O$_3$ hollow spheres for the removal of chromium in water.[142] The presence of the liquid/liquid interface played a significant role along with PVP in the development of hierarchical hollow spheres consisting of single-crystalline polyhedral particles. The formation of
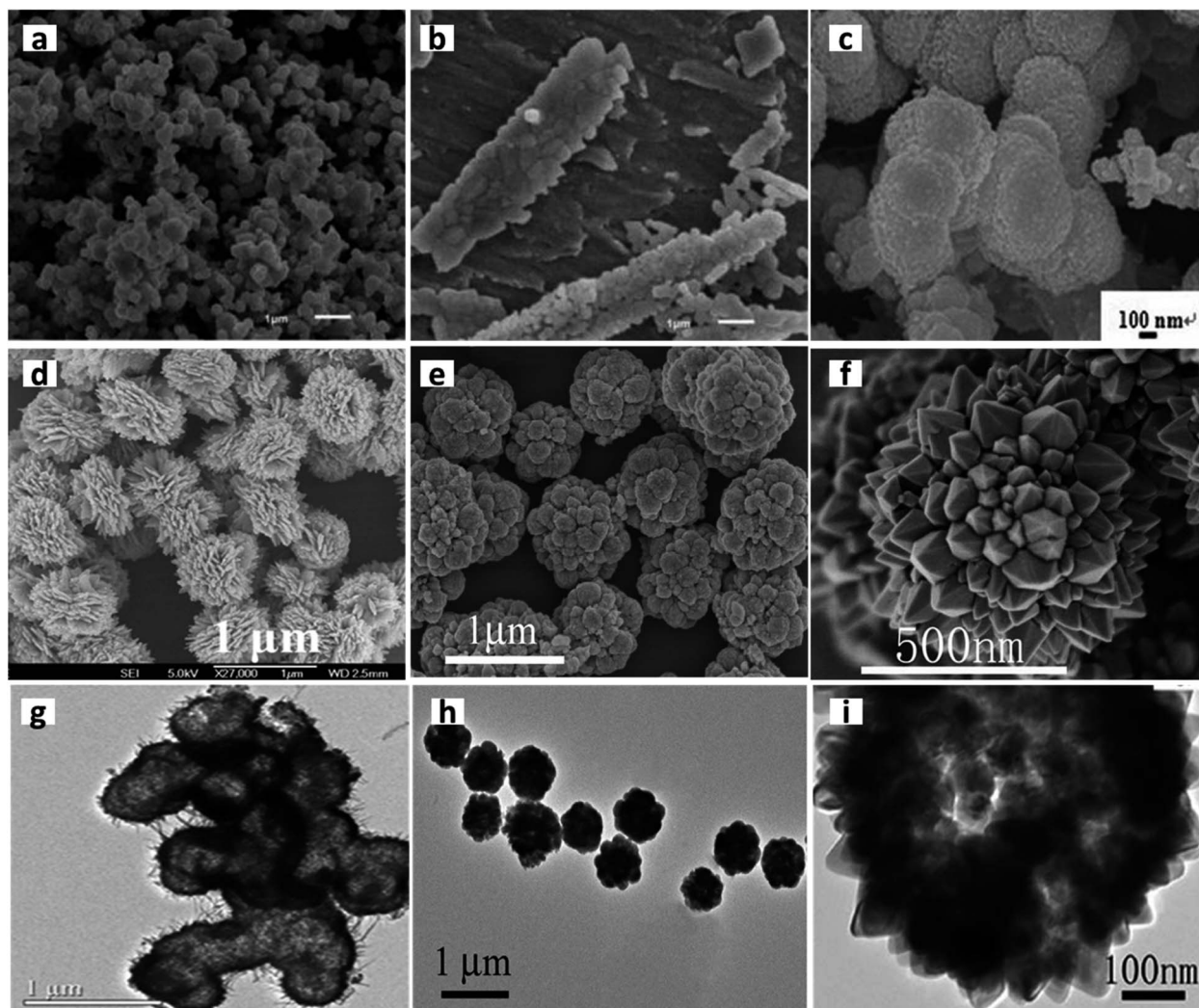
Fig. 12 Typical examples of TMOs with diverse morphologies developed using interface-assisted synthesis. SEM images of (a) MnO nano-particles. Reproduced from ref. 143 with permission from The Royal Society of Chemistry. (b) MnO microbars. Reproduced from ref. 143 with permission from The Royal Society of Chemistry. (c) Urchin-like MnO_2. "Reprinted with permission from ref. 144. Copyright (2014) American Chemical Society." (d) CuO nanospheres. Reprinted from Zhu J. and Qian X., From 2-D CuO Nanosheets to 3-D Hollow Nanospheres: Interface-Assisted Synthesis, Surface Photovoltage Properties and Photocatalytic Activity, *J. Solid State Chem.*, 183, 1632–1639, Copyright (2010), with permission from Elsevier. (e) Cauliflower-like Fe_2O_3. Reprinted from Cheng X. L., Jiang J. Sen, Jin C. Y., Lin C. C., Zeng Y. and Zhang Q. H., Cauliflower-like α-Fe_2O_3 Microstructures: Toluene-Water Interface-Assisted Synthesis, Characterization, and Applications in Wastewater Treatment and Visible-Light Photocatalysis, *Chem. Eng. J.*, 236, 139–148, Copyright (2014), with permission from Elsevier. (f) Durian-like Fe_2O_3. Reproduced from ref. 142 with permission from The Royal Society of Chemistry. TEM images of (g) urchin-like MnO_2. "Reprinted with permission from ref. 144. Copyright (2014) American Chemical Society." (h) Cauliflower-like Fe_2O_3. Reprinted from Cheng X. L., Jiang J. Sen, Jin C. Y., Lin C. C., Zeng Y. and Zhang Q. H., Cauliflower-like α-Fe_2O_3 Microstructures: Toluene−Water Interface-Assisted Synthesis, Characterization, and Applications in Wastewater Treatment and Visible-Light Photocatalysis, *Chem. Eng. J.*, 236, 139−148, Copyright (2014), with permission from Elsevier. (i) Durian-like Fe_2O_3. Reproduced from ref. 142 with permission from The Royal Society of Chemistry.

microrods in the absence of the benzene/water interface affirmed the requirement of the interface for the α-FeOOH to α-Fe_2O_3 phase transformation. Chen *et al.* proposed the tuning of the morphology of MnO by altering the solvent ratio of the *N,N*-dimethylformamide (DMF)/water bisolvent interface.[143] The alteration of the solvent ratio resulted in the formation of four different morphologies, including microrods, 2D flakes, microbars and irregular microparticles, out of which 2D flakes exhibited greater electrochemical activity. Liu *et al.* introduced a facile soft-interface method consisting of a dichloromethane/

water interface for the synthesis of hierarchical mesoporous MnO_2.[144] The as-synthesized MnO_2 exhibited an urchin-like hollow submicrosphere formed by the self-assembly of 1D nanorods at the bisolvent interface. Zhu *et al.* proposed the synthesis of hierarchical CuO hollow nanostructures with enhanced photocatalytic activity.[145] Here, the *n*-octanol/water interface along with the bubble template were used for the assembly of nanosheets into hollow nanostructures, which were formed *via* aggregation followed by the growth mechanism through the bubble template. The use of the liquid/liquid

Table 3   0D, 1D, 2D and 3D TMOs synthesized using different soft-templates

Soft-template category	TMOs	Soft-template used	Dimension	Morphology	Reference
Surfactant	Co_3O_4	Oleic acid	0D	Nanoparticles	147
		CTAB		Nanoparticles	148
		CTAB, PEG	1D	Nanowires	149
		CTAB		Nanorods	149
		CTAB	3D	Flower-like microcrystal	150
	Cr_2O_3	PEG	0D	Nanosphericals	151
		SDS	2D	Nanosheet	
		CTAB		Nanoplates	
	CuO	CTAB	0D	Nanoparticle	152
		CTAB/SDS		Spherical nanoparticles	153
		TOAB	1D	Nanoribbon	113
		PEG		Nanowire bundle	154
		PEG		Belt-like	155
		CTAB		Bamboo leaf-like	
		$Cu(DS)_2$	2D	Leaf-like	156
		Triton-X		Yarn balls	157
		PVA		Cabbage slash	
		SDBS	3D	Butterfly-like	158
	Cu_2O	CTAB	0D	Hollow sphere	159
		CTAB	1D	Nanobelt	160
		CTAB		Nanowhiskers	161
		SDS		Nanowire	162
		CTAB	3D	Rose-like nanoflower	163
		CTAB		Nanoflower	164
	Fe_2O_3/Fe_3O_4	CTAB/PVP/SDBS	0D	Nanoparticle	165
		SDBS		Nanoparticle	166
		CTAB	1D	Nanowire	167
		TEAOH		Nanorod	168
		SDS	2D	Nanolamellar	169
		TETA	3D	Nanoflower	170
	$MnO_2/Mn_3O_4/Mn_2O_3$	CTAB/PVP	0D	Nanocrystals	115
		CTAB		Nano hollow sphere	171
		CTAB		Nanoparticle	172
		PEG	1D	Nanorod	173
		SDS		Nanorod	174
		PVP		Nanofiber	175
		SDBS		Nanowire	176
		CTAB		Nanorod	177
		SDS	2D	Nanosheet	178
		PVP	3D	Birnessite	179
		Oleylamine		3D sphere	180
		SDS		Colloidal sphere	181
		CTAB		Microflower	182
		SDS		Sea-urchin	183
	MoO_2/MoO_3	PEG	0D	Sub-micron sphere	184
		PEG		Hollow microsphere	185
		CTAB/chitosan	1D	Nanorod	186
		SDS		Nanoneedle	187
		SDS		Nanorod	188
		Cetyl alcohol		Nanobelt	189
		Gemini surfactant	2D	Lamellar	190
		CTAB		Microbelt	186
		CTAB	3D	Urchin	191
		PVP		Flake-flower	192
		CTAB		Flower	193
		CTAB		Nest-like	194
		PEG		Porous sponge	195
	NiO	CTAB	0D	Spherical particles	196
		CTAB/Triton-X		Ball-like	197
		PEG		Microsphere	198
		PEG		Nanoparticle	199
		PEG	1D	Rod-like	196
		CTAB		Pine-cone	200

Table 3 (Contd.)

Soft-template category	TMOs	Soft-template used	Dimension	Morphology	Reference
		SDS		Nanotubule	201
		SDS	2D	Nanoflake	197
		P123		Nanosheet	202
		SDS	3D	Hexagonal	196
		SDS		Microflower	203
		PVP		Nanoflower	204
	TiO$_2$	PEG	0D	Nanocrystal	112
		CTAB/PEG		Particles	205
		CTAB		Nanoparticles	206
		PEG/PVP		Nanocrystal	
		CTAB	1D	Nanofiber	207
		CTAB		Nanorod	208 and 209
		PEG		Nanowire	210
		TBAOH	2D	Nanosheet	114
		DDA		Nanosheet	211
		CTAB		Nanosheet	212
		CTAB	3D	Dendrites	213
		CTAB		Nanoflower	214
		PEG		3D mesoporous	215
	VO$_2$/V$_2$O$_5$	CTAB	0D	Nanoparticle	216
		CTAB	1D	Nanobelt	103
		CTAB		Nanorod	216
		PVP		Nanowire	217
		Brij 30		Nanoribbon	218
		Triton-X		Nanowire	
		PVP		Nanorod	219
		PEG		Nanobelt	220
		LAHC	2D	Nanosheet	221
		CTAB		Nanosheet	222
		Cetyl alcohol		Nanoflake	189
		PVP	3D	Hollow microsphere	106 and 223
		PVP/CTAB/SDS/SDBS		Turbine-like structure	224
		PVP		Hydrogel	217
		PVP		Flower-like	225
		SDS		3D network	226
	WO$_3$	CTAB	1D	Nanorod	227 and 228
		HTAB/PEG	2D	Thin film	229
		PEG		Nanosheet	227
		Triton-X		Disc-shaped	230
		CTAB		Nanoplates	231
		CTAB	3D	Microflower	102
		CTAB		Urchin-like	232
	ZnO	CTAB	0D	Nanoparticles	104
		PVP	1D	Nanobelt	107
		Sodium oleate/hydrazine hydrate		Nanorod	233
		CTAB		Nanotube	234
		CTAB		Pencil-like nanorod	235
		PEG		Nanowire	236
		PEG		Micro/nanorod	237
		SDS/PEG		Nanorod	238
		SDS		Needle-like	239
		SDS	2D	Nanosheet	240
		CTAB		Nanoflake	241
		Oleic	3D	Flower-like	242
		SDS/PEG		Flower-like microsphere	240
		Triton-X		Flower-like	243
		PEG/PVP		Multigonal star-shape	244
		CTAB		Flower-like	245
		SDS		Flower-like	246
Block copolymer	Co$_3$O$_4$	P123	0D	Nanocrystals	247
		PS-PMA-PEG		Hollow nanosphere	248
		P123	1D	Channel structure	249
		P123	2D	Nanosheet	250 and 251

Table 3 (Contd.)

Soft-template category	TMOs	Soft-template used	Dimension	Morphology	Reference
	CuO/Cu_2O	P123	0D	Mesoporous spheres	252
		PS-b-PAA-b-PEG		Hollow nanosphere	253
		P123	1D	Nanowire bundle	254
		P123		Nanowire	255
	Fe_2O_3/Fe_3O_4	PS-b-PEO	0D	Nanodot	256
		F127		Spherical nanoparticles	165
		PEO-PPO-PEO		Mesoporous spheres	257
		F127		Hollow microsphere	258
		Cellulose-g-(PAA-b-PS)	1D	Nanorod	259
		PIB-PEO	2D	Film	260
		P123		Rhombohedral	261
		P123	3D	Nanorose	262
	$MnO_2/Mn_3O_4/Mn_2O_3$	P123	0D	Particles	263
		Pebax2533		Nanoparticles	264
		P123	1D	Nanorod	263
		P123		Nanowire	265
		PMPEGMA-b-PBA	2D	Film	266
		P123	3D	Spherical particle	267
		F127		Urchin-like	268
		F127		Flower-like	268
	MoO_2/MoO_3	PS-PMAPTAC-PEO	0D	Hollow nanosphere	269
		PS-b-PVP-b-PEO	1D	Nanotube	270
		KLE	2D	Film	121
	NiO	P123	0D	Nanoparticles	271
		PS-b-P2VP	2D	Film	272
	TiO_2	PS-b-P4VP	0D	Nanoparticles	273
		PDMAEMA-b-PFOMA		Nanoparticles	274
		F127		Microspheres	275
		PS(46)-PMMA(21)	1D	Nanorod	276
		PS-b-P4VP		Needle-like	277
		P123		Hollow fiber	278
		PS(80)-PMMA(80)	2D	Nanowall	276
		P123		Nanosheet	279, 280 and 281
		P123/F127		Thin film	282
	WO_3	PS-PMAPTAC-PEO	0D	Hollow nanosphere	269
		PS-b-PAA		Nanosphere	283
		PS-b-P4VP	1D	Nanowire	284
		P123	2D	Nanosheet	285 and 286
		F127	3D	3D nanowall	287
		$PtBA_{45}PS_{92}PEO_{117}$		Peanut-shaped	288
	ZnO	PS-b-PAA	0D	Nanoparticles	289
		PS-b-P2VP		Nanoparticles	290
		P123	1D	Nanotube	291
		PEO-b-PPO		Biprimatic shape	292
		PEO-b-PPO		Nanorod	293
		PS-b-P4VP	2D	Quasi hexagonally packed nanorings	294
		F127	3D	Flower-like	295
Biological templates	Co_3O_4	Bacteria	1D	Hollow rod	130
		Bacteria	3D	Flower-like microsphere	132
	Cu_2O	Yeast	0D	Hollow microsphere	139
		DNA	1D	Nanowire	128
		Bacterial cellulose	3D	Microtube lattices	296
	Fe_2O_3/Fe_3O_4	Protein	0D	Nanoparticles	126
	$MnO_2/Mn_3O_4/Mn_2O_3$	Bacteria	1D	Rods	131
		DNA		Wire-like	129
		Virus		Nanowire	137
		DNA	2D	Flake-like	129
		Protein		Nanoflake	127
	NiO	L-Cysteine	0D	Spherical hedgehog	297
		Virus	1D	Nanorod	135
		Fungi		Microtube	298
	TiO_2	Alginate	0D	Nanoparticles	299
		Nanocrystalline cellulose		Nanoparticles	300

Table 3 (*Contd.*)

Soft-template category	TMOs	Soft-template used	Dimension	Morphology	Reference
		Protein fibrils	1D	Nanowire	301
	V_2O_5	Yeast	0D	Nanoparticles	302
	WO_3	Protein	1D	Nanofiber	125
	ZnO	Bacterial cellulose	0D	Nanoparticles	133
		Virus	1D	Nanowire	136
		Rice	2D	Flake	303
Interface	CuO	*n*-Octanol/water	3D	Hollow nanosphere	145
	Fe_2O_3	Benzene/water	3D	Durian-like microsphere	142
		Toluene/water		Cauliflower-like	304
	MnO/MnO_2	DMF/water	0D	Nanoparticle	143
				Microbar	143
				Flake	143
		CH_2Cl_2/water	3D	Urchin-like	144
	ZnO	Water/air	2D	Nanosheet	141

interface has also been extended to the formation of mixed TMOs. Our group has developed a bi-solvent interface-assisted synthesis mechanism for the preparation of one of the important mixed TMOs, nickel cobaltite.[146] Here, the *n*-butanol/water interface was employed for the synthesis of 1 nm thick flake-like nickel cobaltite with a single unit cell. The effect of the variation of the *n*-butanol/water solvent ratio on the morphology of the mixed TMOs was also studied in detail, where it was proved that

the 1 : 1 solvent ratio predominates in the morphology and physicochemical properties. Though the interface-assisted method for the fabrication of TMOs is less investigated, it is a promising technique for the future synthesis of TMOs.

A consolidated list of TMOs synthesized in the last decade using different soft-templates along with their morphology tuning is presented in Table 3.
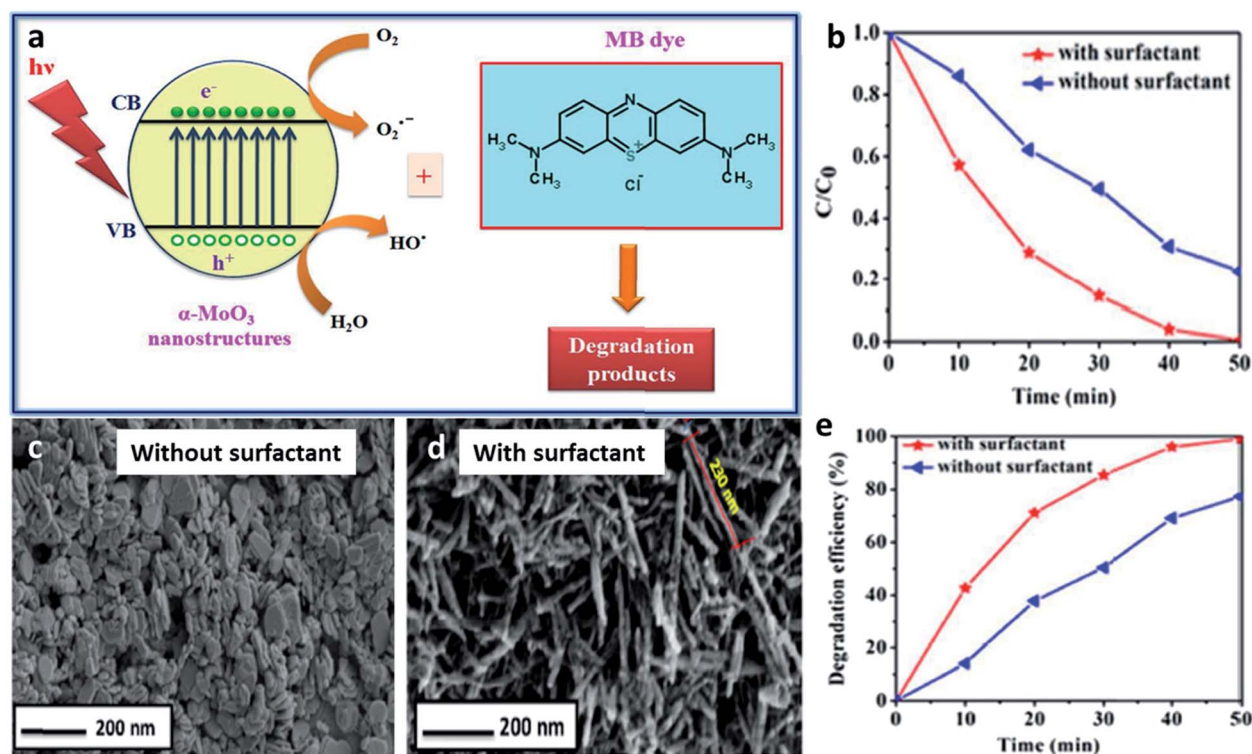
Fig. 13 (a) Schematic representation of the degradation of MB dye using α-MoO₃ nanostructures. Photocatalytic degradation of MB dye solution over synthesized α-MoO₃ nanostructures. (b) Curves of C/C_0 *versus* time interval. (e) Degradation efficiency *versus* time. FESEM images of α-MoO₃ (c) nanoplates and (d) nanoneedles. Reprinted from Rathnasamy R. and Alagan V., A Facile Synthesis and Characterization of α-MoO₃ Nanoneedles and Nanoplates for Visible-Light Photocatalytic Application, *Phys. E*, **102**, 146–152, Copyright (2018), with permission from Elsevier.

Fig. 14 SEM images of (a) monodispersed MoO_3 nanobelts synthesized without the use of surfactants; (b) nest-like MoO_3 synthesized using CTAB, (c) ethanol concentration *vs.* response property at 340 °C. Blue lines represent nest-like MoO_3 and red lines represent monodispersed MoO_3 nanobelts. Reprinted from Li T., Zeng W., Zhang Y. and Hussain S., Nanobelt-Assembled Nest-like MoO_3 Hierarchical Structure: Hydrothermal Synthesis and Gas-Sensing Properties, *Mater. Lett.*, **160**, 476–479, Copyright (2015), with permission from Elsevier. SEM images of (d) ZnO nanosheets synthesized *via* the precipitation method and (e) ZnO nanorods synthesized using CTAB. (f) The effects of respective ZnO nanostructures on the response of 40 ppm NO_2. Reprinted from Bai S., Liu X., Li D., Chen S., Luo R. and Chen A., Synthesis of ZnO Nanorods and Its Application in NO_2 Sensors, *Sens. Actuators, B*, **153**, 110–116, Copyright (2011), with permission from Elsevier.

5. Applications of TMOs synthesized *via* soft-templates

Over the last few decades, TMO materials have been broadly explored as noteworthy materials for a wide range of applications. The unique characteristics possessed by TMOs such as exquisite electrochemical activity, easy availability, wider band gaps and environmental compatibility render them the ability to serve as a promising candidate for a large number of applications. The soft-template-assisted method aids the synthesis of TMOs with desired properties such as controlled pore size, crystallinity and phase.[45] TMOs designed using soft-templates maintain well-defined crystal shapes, thereby enhancing their activity towards various applications to a greater extent.[154] The mesoporous structure synthesized by the use of soft-templates induces higher surface area and structure stability, which are the major requirements for various applications such as catalysis and electrochemical applications.[305] However, controlling the shape and structure of the synthesized TMOs is rather important for tuning the exposed facets for facilitating different applications and soft-template-assisted synthesis has proved to be an important synthesis strategy for the development of shape and structure controlled TMOs.[212] Some of the far-reaching applications of TMOs synthesized *via* soft-template are discussed briefly below:

5.1 Catalysis

One of the most researched applications that focus on the intrinsic properties of TMOs is catalysis, including photocatalysis and electrocatalysis. Various TMOs with diverse morphologies have been employed as catalysts, among which TiO_2 is the most abundant TMO to be used as a catalyst. TiO_2 materials with different morphologies synthesized by using different surfactants have been used for the photocatalytic degradation of many dyes. CTAB-assisted synthesis has resulted in the formation of diverse morphologies such as nanosheets, nanoflowers and nanorods, which have been used for the photocatalytic degradation of azo dyes,[212] rhodamine[214] and for the photodecomposition of wastewater,[208] respectively. The photocatalytic degradation of azo dye has also been studied by Patil *et al.* using a block copolymer F127-assisted synthesis of TiO_2 films.[305] Zhang *et al.* synthesized TiO_2 nanowires using the surfactant PEG for the photocatalytic degradation of a hazardous herbicide, atrazine which is released into the soil.[210] CuO is another highly studied material for catalytic applications. Rao *et al.* studied the effects of two different surfactants, CTAB and SDS on the morphology of CuO nanoparticles and its ability in the photocatalytic degradation of methylene blue.[306] CuO nanowire bundles were prepared by Li *et al.* using PEG for the photodegradation of rhodamine.[154] Certain other surfactant-assisted synthesized TMOs used for catalytic applications include Mn_3O_4 nanorods[173] and α-MoO_3

nanoneedles[187] for the catalytic degradation of methylene blue. A schematic representation of the degradation of methylene blue dye using α-MoO$_3$ and the influence of the surfactant in the catalytic activity is provided in Fig. 13. Bai *et al.* studied the effect of the surfactants CTAB and PEG on the synthesis of Co$_3$O$_4$ for the catalytic combustion of toluene.[149] Apart from the surfactant, the interface has also been used as a soft-template for the synthesis of TMOs for catalytic applications. Cheng *et al.* synthesized flower-like Fe$_2$O$_3$ using a toluene–water interface for the for the effective photocatalytic degradation of rhodamine B.[304]

5.2 Sensors

TMOs have been used as effective sensors for the trace detection of large numbers of molecules. One of the important sensing applications of TMOs is comprised of the gas and humidity sensing. A plethora of research has been conducted in this field for the development of novel materials with the lowest detection limits. The major contribution in the field of gas sensing comes from molybdenum oxides. Various morphologies of molybdenum oxides have been developed using different soft-templates for the gas sensing application. As a reference, Xia *et al.* synthesized nanorod-assembled MoO$_3$ sponges with the aid of the surfactant PEG with enhanced gas sensing properties toward ethanol.[195] The gas sensing ability towards ethanol has also been studied using other molybdenum oxides. MoO$_2$ sub-

micron spheres synthesized using PEG,[184] flower-like MoO$_3$ synthesized using PVP,[192] and nest-like MoO$_3$ synthesized using CTAB[194] were used as effective gas sensors with a high response towards ethanol (Fig. 14a–c). Some other surfactant-assisted synthesized TMOs gas sensors towards ethanol sensing include flower-like NiO synthesized using PVP,[204] urchin-like WO$_3$ synthesized using CTAB,[232] and ZnO nanorods synthesized using SDS/PEG.[238] Another important analyte in the gas sensing application is nitrogen oxide (NO$_x$). Cao *et al.* prepared 3D rose-like Cu$_2$O gas sensors using CTAB for the effective detection of NO$_2$.[163] MoO$_3$ nanorods were fabricated by Bai *et al.* using SDS for the selective detection of NO$_2$.[188] The sensing activity towards NO$_x$ was also studied by Mehta *et al.* using WO$_3$ nanoplates synthesized using CTAB.[231] 1D ZnO nanorods were also employed for the detection of NO$_2$, where ZnO nanorods synthesized using CTAB surfactant showed an enhanced response as compared to the ZnO nanosheets synthesized *via* the precipitation method (Fig. 14d–f).[235] Nanocrystalline CuO was used as an efficient material for the sensing of ammonia gas. As an example, Bedi *et al.* studied the impact of the addition of CTAB on the preparation of thick CuO films for ammonia sensing.[152] Their group also extended their studies to the use of other surfactant materials for the synthesis. In one study, they compared the role of SDS with that of CTAB in the effective sensing of ammonia and concluded that CuO prepared using CTAB surfactant showed a greater kinetic response towards ammonia.[153] TMOs have also been used for various
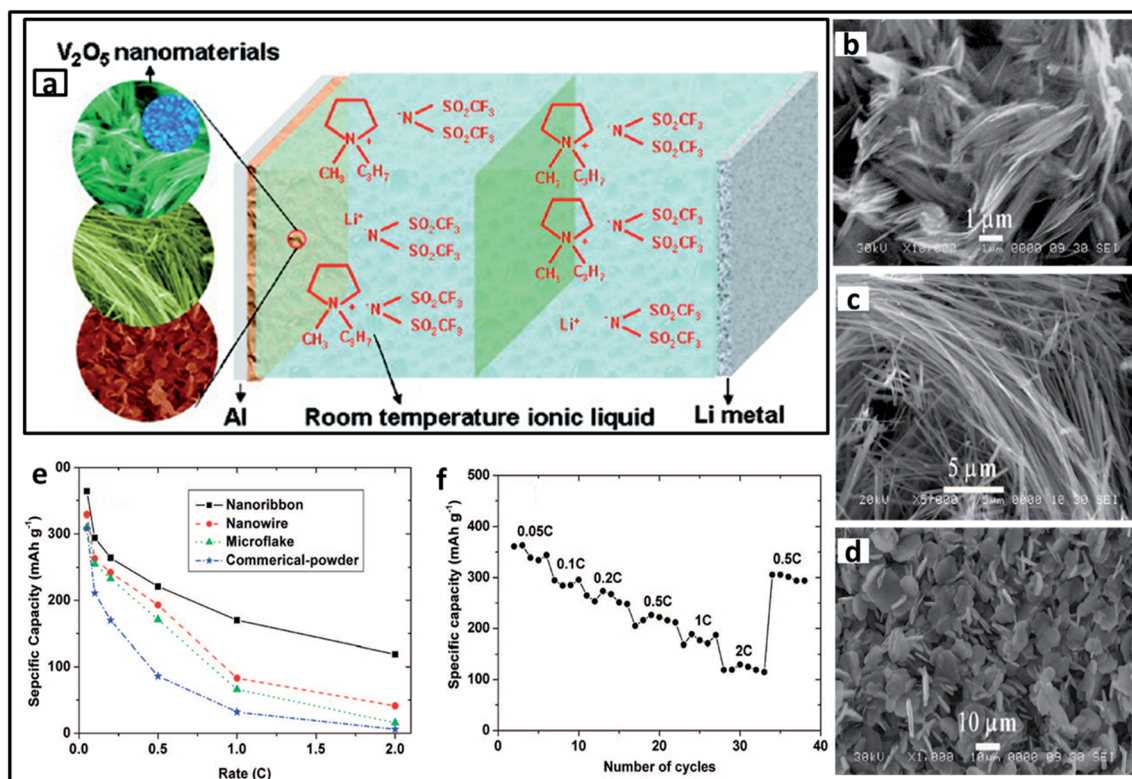

Fig. 15 (a) Schematic representation of a lithium metal battery using V$_2$O$_5$ nanomaterials and room temperature ionic liquid electrolyte. SEM images of diverse morphologies of V$_2$O$_5$ materials: (b) nanoribbons (c) nanowires (d) microflakes and their corresponding (e) specific capacities; (f) cycle life of V$_2$O$_5$ nanoribbon. "Adapted with permission from ref. 218. Copyright (2008) American Chemical Society."

types of humidity sensing. Gong *et al.* fabricated TiO$_2$ nanosheets with increased surface area and surface defects with the aid of P123 for the electrochemical detection of humidity.[280] Parthibavarman *et al.* compared the sensing activity of WO$_3$ with different morphologies towards humidity, and concluded that WO$_3$ nanosheets prepared using PEG are preferred to the nanorods prepared using CTAB.[227] The use of TMOs as sensors in biomedical applications has also gained major attention. TMOs have been used for the trace detection of various biomolecules, pathogens, and toxic compounds inside the human body. Among these, the detection of glucose has been widely studied in the past decade. Tanaka *et al.* reported mesoporous iron oxide synthesized using a block copolymer for both the colorimetric and electrochemical detection of glucose with a good detection limit.[122] TMO nanostructures fabricated with the aid of biological templates were also used for the detection of glucose. For example, NiO prepared using L-cysteine[297] and MnO$_2$ nanowires synthesized using M13 phages[137] were used for the successful selective and reproducible electrochemical detection of glucose. Studies were also conducted on the detection of toxic materials and pathogens in the human body. Zhu *et al.* came out with an effective chemiresistive sensor based on mesoporous WO$_3$ for the detection of a foodborne pathogen *Listeria monocytogenes*.[123] Ding *et al.* developed an amperometric sensor based on porous Mn$_2$O$_3$

nanofibres for the trace detection of one of the toxic compounds, hydrazine.[175] Kim *et al.* introduced an excellent sensor based on WO$_3$ nanofibres for the highly selective and ultra-trace detection of 10 different biomarker gases in the exhaled breath, which is a promising step in fabricating practical exhaled breath monitoring sensors.[125]

5.3 Lithium ion batteries (LIB)

In light of the expeditious growth of the world economy, energy production and storage has become a critical issue. LIB is one of the leading candidates for energy storage, and developing electrodes with greater efficiency is a challenge. Of the numerous materials designed as electrodes for LIB, TMOs have been considered as competent materials owing to their excellent electrochemical performance. Vanadium oxides have gained greater attention in this area owing to their increased theoretical capacity, superior structural flexibility and reduced cost. Nanorod and flower-like VO$_2$ were developed by two different groups using the surfactant PVP as the cathode in LIB.[219,225] Diverse nanostructures of V$_2$O$_5$ were also used as electrode materials for LIB. Cao *et al.* synthesized hollow V$_2$O$_5$ microspheres using PVP,[223] and Chou *et al.* synthesized V$_2$O$_5$ with divergent morphologies using various types of surfactants, of which nanoribbons synthesized using Brij 30 served as an effective cathode material for LIB (Fig. 15).[218] Dai *et al.*
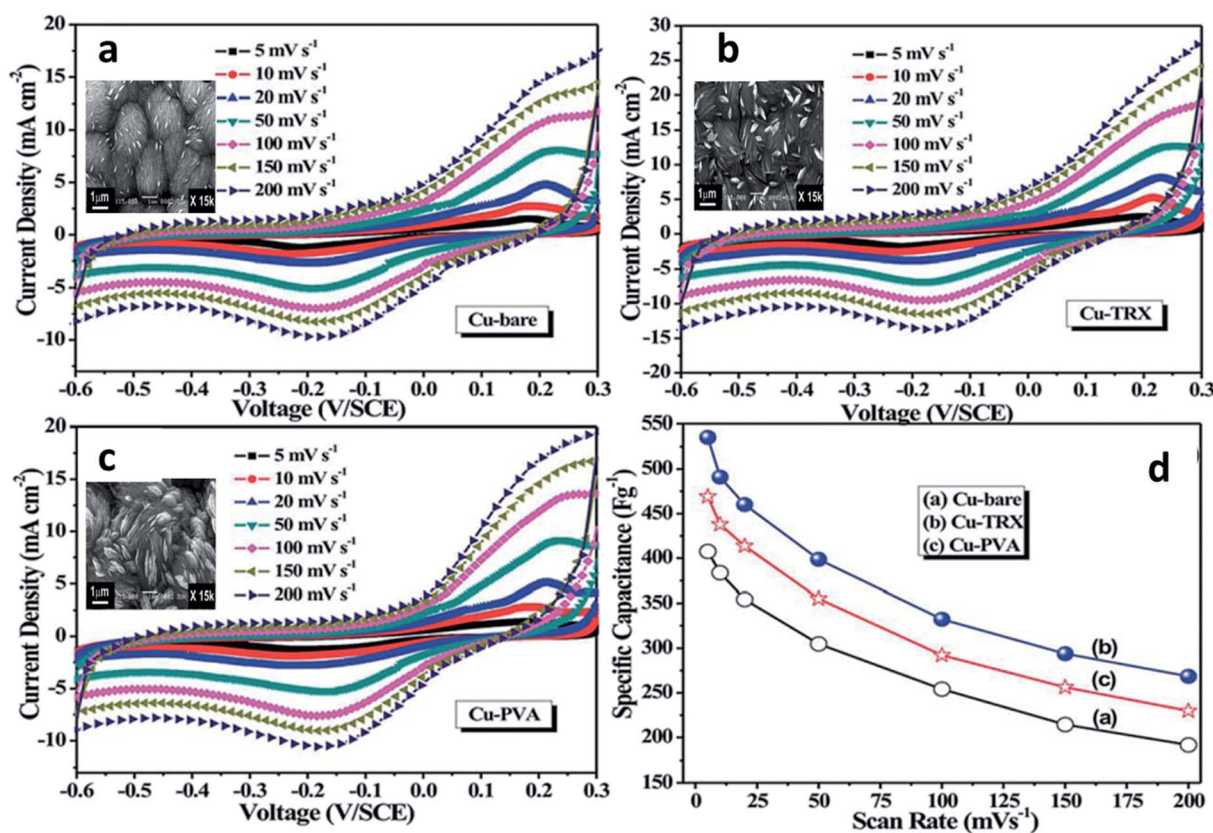

Fig. 16 Cyclic voltammograms of CuO: (a) Cu-bare, (b) Cu-TRX, and (c) Cu-PVA samples at different scan rates. The insets show their corresponding morphologies. (d) Plots of specific capacitance *versus* potential scan rates for corresponding CuO samples. Adapted from ref. 157 with permission from The Royal Society of Chemistry.
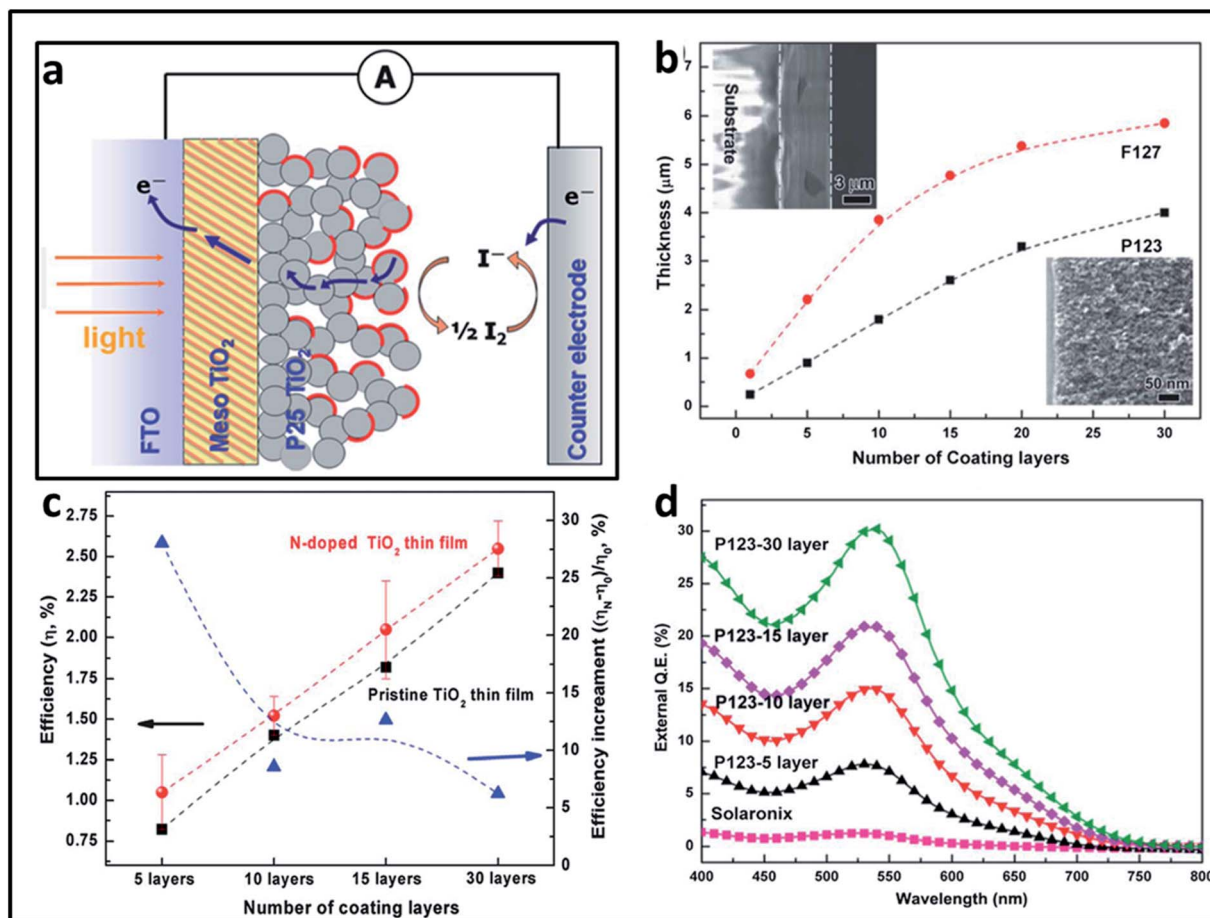
Fig. 17 (a) Schematic diagram of a dye-sensitized solar cell with a bifunctional photoanode consisting of a highly ordered mesoporous thin film and a scattering layer. (b) The thickness of P123 and F127-templated mesoporous TiO_2 thin-films as a function of the number of coatings; the insets present the low and high magnification cross-sectional images of a 30-layer P123-templated mesoporous thin film. (c) Photoconversion efficiency and the efficiency enhancement of solar cells with N-doped mesoporous TiO_2 thin film photoanodes. (d) Incident photon-to-current quantum conversion efficiency (IPCE) spectra of the solar cells with photoanodes consisting of P123-templated mesoporous TiO_2 thin films and Solaronix TiO_2 nanoparticle thin film. Reproduced from ref. 282 with permission from The Royal Society of Chemistry.

composited a 3D $H_3V_3O_8$ hydrogel with carbon nanotubes (CNT) to form $H_3V_3O_8$/CNT film, which served as an excellent electrode material.[217] Other examples of surfactant-assisted synthesized TMOs that serve as the anode material for LIB include Co_3O_4 hollow nanospheres,[248] 3D flower-like Mn_3O_4,[182] and mesoporous TiO_2.[206]

5.4 Supercapacitors

Supercapacitors are another significant solution for the energy storage challenges faced by the present generation. Owing to their increased capacitance, TMOs have been considered as efficient materials for supercapacitors. Various reports are available on the fabrication of TMOs using soft-templates for supercapacitor applications. Different oxides of manganese synthesized with the aid of surfactants were reported with diverse morphologies for competent supercapacitor applications.[171,172,176–178,180] NiO is also an important electrode material for supercapacitor applications. Zhang et al. synthesized 2D NiO nanosheets with the aid of P123 to exhibit higher capacitance.[202]

Ci et al.[203] and Meher et al.[200] studied the effects of specific morphologies on the super capacitance behaviour of NiO. Porous Co_3O_4 synthesized with the aid of both block copolymers[247] and bacteria templates[132] were also reported for higher supercapacitance with excellent cycling stability. Gund et al. examined the process-structure–property relationship of two different morphologies of CuO synthesized using different surfactants.[157] As shown in Fig. 16, the CuO synthesized using Triton-X showed an increased specific capacitance when compared to the other samples. The effects of morphology on the capacitance activity was also stressed by Brezesinski et al.[121] and Panigrahi et al.[226] in their studies on mesoporous MoO_3 and 3D network of V_2O_5, respectively.

5.5 Solar cells

The depletion of fossil fuels has resulted in extended research in the area of renewable energy sources, and solar energy affords an effective solution to deal with the energy crisis. The fabrication of high-efficiency solar cells has been a challenge for

researchers and various materials including TMOs have been developed for solar cell applications. Kim synthesized NiO using the PEG-assisted sol–gel method, which can serve as an excellent pathway for hole transport in organic solar cells.[199] On the other hand, Seo et al. developed TiO_2 nanostructures using a block copolymer that can function as an electron transport layer for the enhanced efficiency of the solar cells.[276] Compared to the silicon-based solar cells, dye-sensitized solar cells are a promising alternative for next-generation energy devices. Sun et al. fabricated different 1D TiO_2 photoanodes for facilitating improved energy conversion in dye-sensitized solar cells, and compared the impact of morphology on the efficiency of energy conversion.[209] They further modified TiO_2 anodes via nitrogen-doping and the top-coating technique to improve the efficiency of the fabricated solar cell (Fig. 17).[282]

6. Summary and outlook

TMOs have captivated the attention of researchers across the globe for the past few decades. Owing to their appealing properties and remarkable applications, the research on TMOs has reached its peak. However, the synthesis of TMOs with unique properties for specific applications is a hurdle. Many synthetic approaches have been developed for the facile and one-step synthesis of TMOs, out of which template-assisted methods have gained greater consideration by virtue of their ability to tune the morphology and physicochemical properties. The tedious process of the removal of templates in the case of hard-template-assisted synthesis has resulted in the widespread use of soft-templates for the fabrication of TMOs.

This review has summed up the recent advancements in the soft-template-assisted synthesis of TMOs. A brief description of different synthetic strategies of TMOs highlighting the top and bottom-up approaches is given, followed by a comprehensive depiction of the soft-template assisted methods. The synthesis of TMOs using different categories of soft-templates is explained along with the role of the soft-template in controlling the morphology and other properties of TMOs. It was observed that each type of soft-template has its own mechanism in tailoring TMOs with desired properties. This review mainly focuses on the state-of-the-art research in the soft-template assisted synthesis of TMOs in the last decade. The diverse applications of the TMOs synthesized using soft-templates have also been discussed briefly. It was concluded from the study that the soft-template-assisted synthesis can serve as an outstanding method for the fabrication of TMOs with well-defined properties and the thus prepared TMOs act as promising candidates for various future applications.

Although there has been a significant breakthrough in the property-controlled synthesis of TMOs using soft-templates, certain hurdles such as the product yield and the requirement of post-synthetic methods have hindered their practical application in various fields. Hence, additional consideration needs to be given to more controlled and facile syntheses for future large-scale productions. Among the different classes of soft-templates, the interface-assisted synthesis of TMOs is the least explored and it opens a new area to the researchers to conquer the material science research with novel inventions. The achievements in soft-template assisted synthesis have instilled more eagerness in the researchers to surmount all the hurdles that remain and contribute extensively to the less explored areas. The coming decades will undeniably witness a protracted breakthrough in these aspects.

Author contributions

The manuscript was written through the contributions of all authors. All authors have given approval to the final version of the manuscript.

Funding sources

Conflicts of interest

There are no conflicts to declare.

References

1 Y. Liu, C. Nam Ong and J. Xie, Nanotechnol. Rev., 2016, 5, 1–2.
2 J. H. Myung, K. A. Tam, S. jung Park, A. Cha and S. Hong, Wiley Interdiscip. Rev.: Nanomed. Nanobiotechnol., 2016, 8, 223–239.
3 P. V. Maheshwari and N. Vishal Gupta, Int. J. PharmTech Res., 2012, 4, 1221–1227.
4 Z. L. Wang and W. Wu, Angew. Chem., Int. Ed., 2012, 51, 11700–11721.
5 J. Meyer, S. Hamwi, M. Kröger, W. Kowalsky, T. Riedl and A. Kahn, Adv. Mater., 2012, 24, 5408–5427.
6 P. He, H. Yu, D. Li and H. Zhou, J. Mater. Chem., 2012, 22, 3680–3695.
7 W. T. Hong, M. Risch, K. A. Stoerzinger, A. Grimaud, J. Suntivich and Y. Shao-Horn, Energy Environ. Sci., 2015, 8, 1404–1427.
8 F. Song, L. Bai, A. Moysiadou, S. Lee, C. Hu, L. Liardet and X. Hu, J. Am. Chem. Soc., 2018, 140, 7748–7759.
9 D. Kim, S. H. Kang, M. Slater, S. Rood, J. T. Vaughey, N. Karan, M. Balasubramanian and C. S. Johnson, Adv. Energy Mater., 2011, 1, 333–336.
10 M. Gutowski, J. E. Jaffe, C. L. Liu, M. Stoker, R. I. Hegde, R. S. Rai and P. J. Tobin, Appl. Phys. Lett., 2002, 80, 1897–1899.
11 J. Robertson, Rep. Prog. Phys., 2006, 69, 327–396.
12 M. Lee, S. Han, S. H. Jeon, B. H. Park, B. S. Kang, S. Ahn, K. H. Kim, C. B. Lee, C. J. Kim, I. Yoo, D. H. Seo, X. Li, J. Park, J. Lee and Y. Park, Nano Lett., 2009, 9, 1476–1481.
13 G. Mavrou, S. Galata, P. Tsipas, A. Sotiropoulos, Y. Panayiotatos, A. Dimoulas, E. K. Evangelou, J. W. Seo and C. Dieker, J. Appl. Phys., 2008, 103, 014506.
14 K. Chen, A. T. Bell and E. Iglesia, J. Catal., 2002, 209, 35–42.

15 M. Kröger, S. Hamwi, J. Meyer, T. Riedl, W. Kowalsky and A. Kahn, *Org. Electron.*, 2009, **10**, 932–938.

16 A. V. Emeline, G. V. Kataeva, A. V. Panasuk, V. K. Ryabchuk, N. V. Sheremetyeva and N. Serpone, *J. Phys. Chem. B*, 2005, **109**, 5175–5185.

17 W. Deng, X. Ji, Q. Chen and C. E. Banks, *RSC Adv.*, 2011, **1**, 1171–1178.

18 Y. Wang, J. Guo, T. Wang, J. Shao, D. Wang and Y. W. Yang, *Nanomaterials*, 2015, **5**, 1667–1689.

19 M. Zheng, X. Xiao, L. Li, P. Gu, X. Dai, H. Tang, Q. Hu, H. Xue and H. Pang, *Sci. China Mater.*, 2018, **61**, 185–209.

20 P. Yu, X. Zhang, Y. Chen and Y. Ma, *Mater. Lett.*, 2010, **64**, 61–64.

21 M. Zheng, H. Tang, L. Li, Q. Hu, L. Zhang, H. Xue and H. Pang, *Adv. Sci.*, 2018, **5**, 1700592.

22 H. Osgood, S. V. Devaguptapu, H. Xu, J. Cho and G. Wu, *Nano Today*, 2016, **11**, 601–625.

23 R. Marschall and L. Wang, *Catal. Today*, 2014, **225**, 111–135.

24 S. Royer and D. Duprez, *ChemCatChem*, 2011, **3**, 24–65.

25 C. Xie, L. Xiao, M. Hu, Z. Bai, X. Xia and D. Zeng, *Sens. Actuators, B*, 2010, **145**, 457–463.

26 L. Jiang, S. Gu, Y. Ding, F. Jiang and Z. Zhang, *Nanoscale*, 2014, **6**, 207–214.

27 N. Sanpo, C. C. Berndt, C. Wen and J. Wang, *Acta Biomater.*, 2013, **9**, 5830–5837.

28 J. W. Rasmussen, E. Martinez, P. Louka and D. G. Wingett, *Expert Opin. Drug Delivery*, 2010, **7**, 1063–1077.

29 L. Mao, K. Zhang, H. S. On Chan and J. Wu, *J. Mater. Chem.*, 2012, **22**, 1845–1851.

30 R. J. H. J. K. Hedlund Orbeck, *J. Vac. Sci. Technol., A*, 2020, **38**, 1–6.

31 V. Chakrapani, M. Brier, A. Puntambekar and T. Digiovanni, *J. Mater. Res.*, 2016, **31**, 17–27.

32 A. C. Papageorgiou, N. S. Beglitis, C. L. Pang, G. Teobaldi, G. Cabailh, Q. Chen, A. J. Fisher, W. A. Hofer and G. Thornton, *Proc. Natl. Acad. Sci. U. S. A.*, 2010, **107**, 2391–2396.

33 Z. Sun, T. Liao, Y. Dou, S. M. Hwang, M. S. Park, L. Jiang, J. H. Kim and S. X. Dou, *Nat. Commun.*, 2014, **5**, 1–9.

34 M. Naguib, O. Mashtalir, M. R. Lukatskaya, B. Dyatkin, C. Zhang, V. Presser, Y. Gogotsi and M. W. Barsoum, *Chem. Commun.*, 2014, **50**, 7420–7423.

35 B. Liu, H. M. Chen, C. Liu, S. C. Andrews, C. Hahn and P. Yang, *J. Am. Chem. Soc.*, 2013, **135**, 9995–9998.

36 X. Xia, Y. Zhang, D. Chao, C. Guan, Y. Zhang, L. Li, X. Ge, I. M. Bacho, J. Tu and H. J. Fan, *Nanoscale*, 2014, **6**, 5008–5048.

37 Z. Sun, T. Liao and L. Kou, *Sci. China Mater.*, 2017, **60**, 1–24.

38 M. A. Khalily, H. Eren, S. Akbayrak, H. H. Susapto, N. Biyikli, S. Özkar and M. O. Guler, *Angew. Chem., Int. Ed.*, 2016, **55**, 12257–12261.

39 M. Roy, S. Ghosh and M. K. Naskar, *Phys. Chem. Chem. Phys.*, 2015, **17**, 10160–10169.

40 G. Zhang and X. W. Lou, *Angew. Chem., Int. Ed.*, 2014, **53**, 9041–9044.

41 H. Bin Wu, J. S. Chen, H. H. Hng and X. W. Lou, *Nanoscale*, 2012, **4**, 2526–2542.

42 N. D. Petkovich and A. Stein, *Chem. Soc. Rev.*, 2013, **42**, 3721–3739.

43 L. Zhang, L. Jin, B. Liu and J. He, *Front. Chem.*, 2019, **7**, 1–13.

44 Q. Zhang, H. Y. Wang, X. Jia, B. Liu and Y. Yang, *Nanoscale*, 2013, **5**, 7175–7183.

45 D. Gu and F. Schüth, *Chem. Soc. Rev.*, 2014, **43**, 313–344.

46 Y. Zhang, L. Li, H. Su, W. Huang and X. Dong, *J. Mater. Chem. A*, 2015, **3**, 43–59.

47 Y. Ren and P. G. Bruce, *Chem. Soc. Rev.*, 2012, **41**, 4909–4927.

48 T. Guo, M. Yao, Y. Lin and C. Nan, *CrystEngComm*, 2015, **17**, 3551–3585.

49 J. S. Hu, L. S. Zhong, W. G. Song and L. J. Wan, *Adv. Mater.*, 2008, **20**, 2977–2982.

50 Y. Liu, J. Goebl and Y. Yin, *Chem. Soc. Rev.*, 2013, **42**, 2610–2653.

51 X. Y. Liu, K. X. Wang and J. S. Chen, *Energy Storage Mater.*, 2016, **3**, 1–17.

52 T. Yang, T. T. Song, M. Callsen, J. Zhou, J. W. Chai, Y. P. Feng, S. J. Wang and M. Yang, *Adv. Mater. Interfaces*, 2019, **6**, 1–19.

53 F. Li, G. Parteder, F. Allegretti, C. Franchini, R. Podloucky, S. Surnev and F. P. Netzer, *J. Phys.: Condens. Matter*, 2009, **21**, 1–11.

54 J. Tao, T. Luttrell and M. Batzill, *Nat. Chem.*, 2011, **3**, 296–300.

55 S. Pedireddy, H. K. Lee, W. W. Tjiu, I. Y. Phang, H. R. Tan, S. Q. Chua, C. Troadec and X. Y. Ling, *Nat. Commun.*, 2014, **5**, 1–9.

56 S. Yang, W. Yue, J. Zhu, Y. Ren and X. Yang, *Adv. Funct. Mater.*, 2013, **23**, 3570–3576.

57 G. Zhou, D. W. Wang, L. C. Yin, N. Li, F. Li and H. M. Cheng, *ACS Nano*, 2012, **6**, 3214–3223.

58 C. Zhao, H. Zhang, W. Si and H. Wu, *Nat. Commun.*, 2016, **7**, 1–8.

59 D. Mailly, *Eur. Phys. J.: Spec. Top.*, 2009, **172**, 333–342.

60 J. Mei, T. Liao, L. Kou and Z. Sun, *Adv. Mater.*, 2017, **29**, 1–25.

61 A. Biswas, I. S. Bayer, A. S. Biris, T. Wang, E. Dervishi and F. Faupel, *Adv. Colloid Interface Sci.*, 2012, **170**, 2–27.

62 G. Zhang, X. Xiao, B. Li, P. Gu, H. Xue and H. Pang, *J. Mater. Chem. A*, 2017, **5**, 8155–8186.

63 C. M. Ghimbeu, J. M. Le Meins, C. Zlotea, L. Vidal, G. Schrodj, M. Latroche and C. Vix-Guterl, *Carbon*, 2014, **67**, 260–272.

64 Y. Zhai, Y. Dou, X. Liu, S. S. Park, C. S. Ha and D. Zhao, *Carbon*, 2011, **49**, 545–555.

65 N. Pal and A. Bhaumik, *Adv. Colloid Interface Sci.*, 2013, **189–190**, 21–41.

66 V. M. Prida, V. Vega, J. García, L. Iglesias, B. Hernando and I. Minguez-Bacho, *Electrochemical methods for template-assisted synthesis of nanostructured materials*, 2015.

67 K. Khun, Z. H. Ibupoto, X. Liu, V. Beni and M. Willander, *Mater. Sci. Eng., B*, 2015, **194**, 94–100.

68 L. Peng, P. Xiong, L. Ma, Y. Yuan, Y. Zhu, D. Chen, X. Luo, J. Lu, K. Amine and G. Yu, *Nat. Commun.*, 2017, **8**, 1–10.

69 X. Xiao, H. Song, S. Lin, Y. Zhou, X. Zhan, Z. Hu, Q. Zhang, J. Sun, B. Yang, T. Li, L. Jiao, J. Zhou, J. Tang and Y. Gogotsi, *Nat. Commun.*, 2016, **7**, 1–8.

70 S. Zhu, J. Li, X. Deng, C. He, E. Liu, F. He, C. Shi and N. Zhao, *Adv. Funct. Mater.*, 2017, **27**, 1–8.

71 H. Yang and D. Zhao, *J. Mater. Chem.*, 2005, **15**, 1217–1231.

72 B. Platschek, A. Keilbach and T. Bein, *Adv. Mater.*, 2011, **23**, 2395–2412.

73 G. Kawamura, H. Muto and A. Matsuda, *Front. Chem.*, 2014, **2**, 1–4.

74 H. J. Liu, X. M. Wang, W. J. Cui, Y. Q. Dou, D. Y. Zhao and Y. Y. Xia, *J. Mater. Chem.*, 2010, **20**, 4223–4230.

75 M. Hu, A. A. Belik, M. Imura, K. Mibu, Y. Tsujimoto and Y. Yamauchi, *Chem. Mater.*, 2012, **24**, 2698–2707.

76 S. G. Hosseini, R. Ahmadi, A. Ghavi and A. Kashi, *Powder Technol.*, 2015, **278**, 316–322.

77 A. Ahmed, R. Clowes, P. Myers and H. Zhang, *J. Mater. Chem.*, 2011, **21**, 5753–5763.

78 G. L. Drisko, A. Zelcer, V. Luca, R. A. Caruso and G. J. D. A. A. Soler-Illia, *Chem. Mater.*, 2010, **22**, 4379–4385.

79 C. Mijangos, R. Hernández and J. Martín, *Prog. Polym. Sci.*, 2016, **54–55**, 148–182.

80 A. H. Lu and F. Schüth, *C. R. Chim.*, 2005, **8**, 609–620.

81 A. H. Lu and F. Schüth, *Adv. Mater.*, 2006, **18**, 1793–1805.

82 Y. Meng, D. Gu, F. Zhang, Y. Shi, H. Yang, Z. Li, C. Yu, B. Tu and D. Zhao, *Angew. Chem., Int. Ed.*, 2005, **44**, 7053–7059.

83 W. Li, Z. Wu, J. Wang, A. A. Elzatahry and D. Zhao, *Chem. Mater.*, 2014, **26**, 287–298.

84 H. N. Lokupitiya, A. Jones, B. Reid, S. Guldin and M. Stefik, *Chem. Mater.*, 2016, **28**, 1653–1667.

85 B. P. Bastakoti, Y. Li, S. Guragain, M. Pramanik, S. M. Alshehri, T. Ahamad, Z. Liu and Y. Yamauchi, *Chem. – Eur. J.*, 2016, **22**, 7463–7467.

86 B. P. Bastakoti, S. Ishihara, S. Y. Leo, K. Ariga, K. C. W. Wu and Y. Yamauchi, *Langmuir*, 2014, **30**, 651–659.

87 A. B. D. Nandiyanto, T. Ogi, F. Iskandar and K. Okuyama, *Chem. Eng. J.*, 2011, **167**, 409–415.

88 B. Liu, Z. Luo, A. Federico, W. Song, S. L. Suib and J. He, *Chem. Mater.*, 2015, **27**, 6173–6176.

89 B. Liu, M. Louis, L. Jin, G. Li and J. He, *Chem. – Eur. J.*, 2018, **24**, 9651–9657.

90 L. Jin, B. Liu, M. E. Louis, G. Li and J. He, *ACS Appl. Mater. Interfaces*, 2020, **12**, 9617–9627.

91 B. Liu, L. Jin, H. Zheng, H. Yao, Y. Wu, A. Lopes and J. He, *ACS Appl. Mater. Interfaces*, 2017, **9**, 1746–1758.

92 B. Liu, C. H. Kuo, J. Chen, Z. Luo, S. Thanneeru, W. Li, W. Song, S. Biswas, S. L. Suib and J. He, *Angew. Chem., Int. Ed.*, 2015, **54**, 9061–9065.

93 Y. Wan, Y. Shi and D. Zhao, *Chem. Commun.*, 2007, 897–926.

94 G. J. A. A. Soler-Illia and O. Azzaroni, *Chem. Soc. Rev.*, 2011, **40**, 1107–1150.

95 J. Fan, S. W. Boettcher, C. K. Tsung, Q. Shi, M. Schierhorn and G. D. Stucky, *Chem. Mater.*, 2008, **20**, 909–921.

96 X. Zhang, W. Lu, J. Dai, L. Bourgeois, N. Hao, H. Wang, D. Zhao and P. A. Webley, *Angew. Chem., Int. Ed.*, 2010, **49**, 10101–10105.

97 D. Grosso, F. Cagnol, G. J. D. A. A. Soler-Illia, E. L. Crepaldi, H. Amenitsch, A. Brunet-Bruneau, A. Bourgeois and C. Sanchez, *Adv. Funct. Mater.*, 2004, **14**, 309–322.

98 Q. Huo, D. I. Margolese, U. Ciesla, P. Feng, T. E. Gier, P. Sieger, R. Leon, P. M. Petroff, F. Schüth and G. D. Stucky, *Nature*, 1994, **368**, 317–321.

99 J. Ž. Manojlović, *Therm. Sci.*, 2013, **16**, 631–640.

100 C. Rupp, H. Steckel and B. W. Müller, *Int. J. Pharm.*, 2010, **387**, 120–128.

101 Y. Li, X. Y. Yang, Y. Feng, Z. Y. Yuan and B. L. Su, *Crit. Rev. Solid State Mater. Sci.*, 2012, **37**, 1–74.

102 O. Yayapao, T. Thongtem, A. Phuruangrat and S. Thongtem, *J. Alloys Compd.*, 2011, **509**, 2294–2299.

103 N. Li, W. Huang, Q. Shi, Y. Zhang and L. Song, *Ceram. Int.*, 2013, **39**, 6199–6206.

104 C. Amirthavalli, A. Manikandan and A. A. M. Prince, *Ceram. Int.*, 2018, **44**, 15290–15297.

105 X. Wang, X. L. Wu, Y. G. Guo, Y. Zhong, X. Cao, Y. Ma and J. Yao, *Adv. Funct. Mater.*, 2010, **20**, 1680–1686.

106 C. Cao, Y. Gao, L. Kang and H. Luo, *CrystEngComm*, 2010, **12**, 4048–4051.

107 X. Cao, N. Wang, L. Wang and L. Guo, *J. Nanoparticle Res.*, 2010, **12**, 143–150.

108 D. P. Dubal, W. B. Kim and C. D. Lokhande, *J. Alloys Compd.*, 2011, **509**, 10050–10054.

109 D. P. Dubal, G. S. Gund, R. Holze, H. S. Jadhav, C. D. Lokhande and C. J. Park, *Dalton Trans.*, 2013, **42**, 6459–6467.

110 Y. Zhang, X. Bo, A. Nsabimana, H. Wang, M. Li and L. Guo, *Analyst*, 2013, **138**, 3633–3637.

111 B. Luo, X. Li, X. Li, L. Xue, S. Li and X. Li, *CrystEngComm*, 2013, **15**, 5654–5659.

112 B. Akram, K. Ahmad, J. Khan, B. A. Khan and J. Akhtar, *New J. Chem.*, 2018, **42**, 10947–10952.

113 Y. X. Zhang, M. Huang, M. Kuang, C. P. Liu, J. L. Tan, M. Dong, Y. Yuan, X. L. Zhao and Z. Wen, *Int. J. Electrochem. Sci.*, 2013, **8**, 1366–1381.

114 M. Leng, Y. Chen and J. Xue, *Nanoscale*, 2014, **6**, 8531–8534.

115 P. Zhang, Y. Zhan, B. Cai, C. Hao, J. Wang, C. Liu, Z. Meng, Z. Yin and Q. Chen, *Nano Res.*, 2010, **3**, 235–243.

116 L. Chuenchom, R. Kraehnert and B. M. Smarsly, *Soft Matter*, 2012, **8**, 10801–10812.

117 G. Gaucher, M. H. Dufresne, V. P. Sant, N. Kang, D. Maysinger and J. C. Leroux, *J. Controlled Release*, 2005, **109**, 169–188.

118 P. Yang, D. Zhao, D. I. Margolese, B. F. Chmelka and G. D. Stucky, *Nature*, 1998, **396**, 152–155.

119 P. Yang, D. Zhao, D. I. Margolese, B. F. Chmelka and G. D. Stucky, *Chem. Mater.*, 1999, **11**, 2813–2826.

120 J. Lee, M. Christopher Orilall, S. C. Warren, M. Kamperman, F. J. Disalvo and U. Wiesner, *Nat. Mater.*, 2008, **7**, 222–228.

121 T. Brezesinski, J. Wang, S. H. Tolbert and B. Dunn, *Nat. Mater.*, 2010, **9**, 146–151.

122 S. Tanaka, Y. V. Kaneti, R. Bhattacharjee, M. N. Islam, R. Nakahata, N. Abdullah, S. I. Yusa, N. T. Nguyen,

M. J. A. Shiddiky, Y. Yamauchi and M. S. A. Hossain, *ACS Appl. Mater. Interfaces*, 2018, **10**, 1039–1049.

123 Y. Zhu, Y. Zhao, J. Ma, X. Cheng, J. Xie, P. Xu, H. Liu, H. Liu, H. Zhang, M. Wu, A. A. Elzatahry, A. Alghamdi, Y. Deng and D. Zhao, *J. Am. Chem. Soc.*, 2017, **139**, 10365–10373.

124 X. Zhou, Y. Zhu, W. Luo, Y. Ren, P. Xu, A. A. Elzatahry, X. Cheng, A. Alghamdi, Y. Deng and D. Zhao, *J. Mater. Chem. A*, 2016, **4**, 15064–15071.

125 S. J. Kim, S. J. Choi, J. S. Jang, N. H. Kim, M. Hakim, H. L. Tuller and I. D. Kim, *ACS Nano*, 2016, **10**, 5891–5899.

126 S. Kashyap, T. J. Woehl, X. Liu, S. K. Mallapragada and T. Prozorov, *ACS Nano*, 2014, **8**, 9097–9106.

127 L. Han, H. Zhang, D. Chen and F. Li, *Adv. Funct. Mater.*, 2018, **28**, 1–9.

128 R. Hassanien, S. A. F. Al-Said, L. Šiller, R. Little, N. G. Wright, A. Houlton and B. R. Horrocks, *Nanotechnology*, 2012, **23**, 1–12.

129 S. R. Ede, A. Ramadoss, S. Anantharaj, U. Nithiyanantham and S. Kundu, *Phys. Chem. Chem. Phys.*, 2014, **16**, 21846–21859.

130 H. W. Shim, Y. H. Jin, S. D. Seo, S. H. Lee and D. W. Kim, *ACS Nano*, 2011, **5**, 443–449.

131 H. W. Shim, A. H. Lim, K. M. Min and D. W. Kim, *CrystEngComm*, 2011, **13**, 6747–6752.

132 H. W. Shim, A. H. Lim, J. C. Kim, E. Jang, S. D. Seo, G. H. Lee, T. D. Kim and D. W. Kim, *Sci. Rep.*, 2013, **3**, 1–9.

133 S. Chen, B. Zhou, W. Hu, W. Zhang, N. Yin and H. Wang, *Carbohydr. Polym.*, 2013, **92**, 1953–1959.

134 H. Zhou, T. Fan, J. Ding, D. Zhang and Q. Guo, *Opt. Express*, 2012, **20**, A340.

135 S. Chu, K. Gerasopoulos and R. Ghodssi, *Electrochim. Acta*, 2016, **220**, 184–192.

136 P. Atanasova, D. Rothenstein, J. J. Schneider, R. C. Hoffmann, S. Dilfer, S. Eiben, C. Wege, H. Jeske and J. Bill, *Adv. Mater.*, 2011, **23**, 4918–4922.

137 L. Han, C. Shao, B. Liang and A. Liu, *ACS Appl. Mater. Interfaces*, 2016, **8**, 13768–13776.

138 D. Oh, J. Qi, B. Han, G. Zhang, T. J. Carney, J. Ohmura, Y. Zhang, Y. Shao-Horn and A. M. Belcher, *Nano Lett.*, 2014, **14**, 4837–4845.

139 W. He, X. Tian, Y. Du, C. Sun, X. Zhang, X. Han, S. Han, X. Sun, X. Du and Y. Yue, *Mater. Sci. Eng., C*, 2010, **30**, 758–762.

140 R. Dong, T. Zhang and X. Feng, *Chem. Rev.*, 2018, **118**, 6189–6325.

141 F. Wang, J. H. Seo, G. Luo, M. B. Starr, Z. Li, D. Geng, X. Yin, S. Wang, D. G. Fraser, D. Morgan, Z. Ma and X. Wang, *Nat. Commun.*, 2016, **7**, 1–7.

142 X. L. Cheng, J. Sen Jiang, M. Hu, G. Y. Mao, Z. W. Liu, Y. Zeng and Q. H. Zhang, *CrystEngComm*, 2012, **14**, 3056–3062.

143 Z. Chen, C. Wang, M. Chen, C. Ye, Z. Lin, L. Xing, Y. Liao, M. Xu, G. Cao and W. Li, *J. Mater. Chem. A*, 2019, **7**, 3924–3932.

144 Y. Liu, Z. Chen, C. H. Shek, C. M. L. Wu and J. K. L. Lai, *ACS Appl. Mater. Interfaces*, 2014, **6**, 9776–9784.

145 J. Zhu and X. Qian, *J. Solid State Chem.*, 2010, **183**, 1632–1639.

146 R. Rahman Poolakkandy, S. Kaladi Chondath, N. Puthiyottil, D. Davis and M. M. Menamparambath, *Langmuir*, 2020, **36**, 872–879.

147 F. Mohandes, F. Davar and M. Salavati-Niasari, *J. Magn. Magn. Mater.*, 2010, **322**, 872–877.

148 Y. Wang, J. C. Shi, J. L. Cao, G. Sun and Z. Y. Zhang, *Mater. Lett.*, 2011, **65**, 222–224.

149 G. Bai, H. Dai, J. Deng, Y. Liu, F. Wang, Z. Zhao, W. Qiu and C. T. Au, *Appl. Catal., A*, 2013, **450**, 42–49.

150 W. Wang, J. Wang, J. Xu, Y. Liang, Y. Zhang, Z. Liu and X. Bai, *Mater. Lett.*, 2015, **159**, 293–296.

151 K. Anandan and V. Rajendran, *Mater. Lett.*, 2015, **146**, 99–102.

152 R. K. Bedi and I. Singh, *ACS Appl. Mater. Interfaces*, 2010, **2**, 1361–1368.

153 I. Singh and R. K. Bedi, *Solid State Sci.*, 2011, **13**, 2011–2018.

154 Y. Li, X. Y. Yang, J. Rooke, G. Van Tendeloo and B. L. Su, *J. Colloid Interface Sci.*, 2010, **348**, 303–312.

155 W. Wang, Q. Zhou, X. Fei, Y. He, P. Zhang, G. Zhang, L. Peng and W. Xie, *CrystEngComm*, 2010, **12**, 2232–2237.

156 a. Bello, D. Dodoo-Arhin, K. Makgopa, M. Fabiane and N. Manyala, *Am. J. Mater. Sci.*, 2014, **4**, 64–73.

157 G. S. Gund, D. P. Dubal, D. S. Dhawale, S. S. Shinde and C. D. Lokhande, *RSC Adv.*, 2013, **3**, 24099–24107.

158 Y. Zhang, W. O. Siu, X. Wang, T. Cui, W. Cui, Y. Zhang and Z. Zhang, *Eur. J. Inorg. Chem.*, 2009, 168–173.

159 W. Wang, Y. Tu, P. Zhang and G. Zhang, *CrystEngComm*, 2011, **13**, 1838–1842.

160 X. W. Huang, Z. J. Liu and Y. F. Zheng, *Chin. Chem. Lett.*, 2011, **22**, 879–882.

161 P. Sharma and S. K. Sharma, *J. Alloys Compd.*, 2013, **557**, 152–159.

162 Y. Xiong, Z. Li, R. Zhang, Y. Xie, J. Yang and C. Wu, *J. Phys. Chem. B*, 2003, **107**, 3697–3702.

163 S. Cao, H. Chen, T. Han, C. Zhao and L. Peng, *Mater. Lett.*, 2016, **180**, 135–139.

164 Q. Luo, Y. Li and R. Suqin, *Cryst. Growth Des.*, 2007, **7**, 87–92.

165 H. Ming, J. Ming, S. Oh, S. Tian, Q. Zhou, H. Huang, Y. Sun and J. Zheng, *ACS Appl. Mater. Interfaces*, 2014, **6**, 15499–15509.

166 Y. Xu, S. Yang, G. Zhang, Y. Sun, D. Gao and Y. Sun, *Mater. Lett.*, 2011, **65**, 1911–1914.

167 N. Du, Y. Xu, H. Zhang, C. Zhai and D. Yang, *Nanoscale Res. Lett.*, 2010, **5**, 1295–1300.

168 Z. Zhong, J. Ho, J. Teo, S. Shen and A. Gedanken, *Chem. Mater.*, 2007, **19**, 4776–4782.

169 J. Wang, J. Xu, X. Meng and Y. Huang, *Mater. Res. Bull.*, 2014, **49**, 176–179.

170 R. Ramesh, M. Rajalakshmi, C. Muthamizhchelvan and S. Ponnusamy, *Mater. Lett.*, 2012, **70**, 73–75.

171 H. Zhang, Y. Wang, C. Liu and H. Jiang, *J. Alloys Compd.*, 2012, **517**, 1–8.

172 B. Gnana Sundara Raj, A. M. Asiri, J. J. Wu and S. Anandan, *J. Alloys Compd.*, 2015, **636**, 234–240.

173 Z. Bai, B. Sun, N. Fan, Z. Ju, M. Li, L. Xu and Y. Qian, *Chem. – Eur. J.*, 2012, **18**, 5319–5324.

174 M. Salavati-Niasari, M. Esmaeili-Zare and M. Gholami-Daghian, *Adv. Powder Technol.*, 2014, **25**, 879–884.

175 Y. Ding, C. Hou, B. Li and Y. Lei, *Electroanalysis*, 2011, **23**, 1245–1251.

176 Y. Li, Y. Mei, L. Q. Zhang, J. H. Wang, A. R. Liu, Y. J. Zhang and S. Q. Liu, *J. Colloid Interface Sci.*, 2015, **455**, 188–193.

177 Y. Li, H. Xie, J. Wang and L. Chen, *Mater. Lett.*, 2011, **65**, 403–405.

178 Z. Liu, K. Xu, H. Sun and S. Yin, *Small*, 2015, **11**, 2182–2191.

179 X. Hao, J. Zhao, Y. Song and Z. Huang, *J. Nano Res.*, 2018, **53**, 1–6.

180 G. P. Ojha, A. Muthurasu, B. Dahal, T. Mukhiya, D. Kang and H. Y. Kim, *J. Electroanal. Chem.*, 2019, **837**, 254–265.

181 P. Li, C. Nan, Z. Wei, J. Lu, Q. Peng and Y. Li, *Chem. Mater.*, 2010, **22**, 4232–4236.

182 H. L. Fei and C. Yang, *Res. Rev. J. Mat. Sci.*, 2018, **1**, 1–10.

183 X. C. Song, Y. Zhao and Y. F. Zheng, *Cryst. Growth Des.*, 2007, **7**, 159–162.

184 T. Yunusi, C. Yang, W. Cai, F. Xiao, J. Wang and X. Su, *Ceram. Int.*, 2013, **39**, 3435–3439.

185 Z. Wang, H. Wang, C. Yang and J. Wu, *Mater. Lett.*, 2010, **64**, 2170–2172.

186 Z. Cui, W. Yuan and C. M. Li, *J. Mater. Chem. A*, 2013, **1**, 12926–12931.

187 R. Rathnasamy and V. Alagan, *Phys. E*, 2018, **102**, 146–152.

188 S. Bai, S. Chen, L. Chen, K. Zhang, R. Luo, D. Li and C. C. Liu, *Sens. Actuators, B*, 2012, **174**, 51–58.

189 R. Sowmiyanarayan and J. Santhanalakshmi, *Nano Vis.*, 2012, **2**, 49–60.

190 X. Yu, Z. Xu and S. Han, *J. Porous Mater.*, 2010, **17**, 99–105.

191 Y. Li, T. Liu, T. Li and X. Peng, *Mater. Lett.*, 2015, **140**, 48–50.

192 Y. Li, *Phys. E*, 2017, **94**, 22–24.

193 S. Wang, Y. Zhang, X. Ma, W. Wang, X. Li, Z. Zhang and Y. Qian, *Solid State Commun.*, 2005, **136**, 283–287.

194 T. Li, W. Zeng, Y. Zhang and S. Hussain, *Mater. Lett.*, 2015, **160**, 476–479.

195 Y. Xia, C. Wu, N. Zhao and H. Zhang, *Mater. Lett.*, 2016, **171**, 117–120.

196 V. Rajendran and K. Anandan, *Mater. Sci. Semicond. Process.*, 2015, **38**, 203–208.

197 P. Justin, S. K. Meher and G. R. Rao, *J. Phys. Chem. C*, 2010, **114**, 5203–5210.

198 Z. Zhu, Y. Zhang, Y. Zhang, H. Liu, C. Zhu and Y. Wu, *Ceram. Int.*, 2013, **39**, 2567–2573.

199 J. K. Kim, *Polymers*, 2019, **11**, 1–9.

200 S. K. Meher, P. Justin and G. R. Rao, *Electrochim. Acta*, 2010, **55**, 8388–8396.

201 H. J. Liu, T. Y. Peng, D. Zhao, K. Dai and Z. H. Peng, *Mater. Chem. Phys.*, 2004, **87**, 81–86.

202 L. Zhang, W. Zheng, H. Jiu, C. Ni, J. Chang and G. Qi, *Electrochim. Acta*, 2016, **215**, 212–222.

203 S. Ci, Z. Wen, Y. Qian, S. Mao, S. Cui and J. Chen, *Sci. Rep.*, 2015, **5**, 1–12.

204 Q. Gao, W. Zeng and R. Miao, *J. Mater. Sci. Mater. Electron.*, 2016, **27**, 9410–9416.

205 J. Payormhorm, S. Chuangchote, K. Kiatkittipong, S. Chiarakorn and N. Laosiripojana, *Mater. Chem. Phys.*, 2017, **196**, 29–36.

206 S. Casino, F. Di Lupo, C. Francia, A. Tuel, S. Bodoardo and C. Gerbaldi, *J. Alloys Compd.*, 2014, **594**, 114–121.

207 T. D. Deepa, S. Mohapatra, S. V. Nair, A. S. Nair and A. K. Rai, *Sustainable Energy Fuels*, 2017, **1**, 138–144.

208 B. Sun, X. L. Xu and G. W. Zhou, *Adv. Mater. Res.*, 2014, **918**, 12–16.

209 Z. Sun, J. H. Kim, T. Liao, Y. Zhao, F. Bijarbooneh, V. Malgras and S. X. Dou, *CrystEngComm*, 2012, **14**, 5472–5478.

210 Y. Zhang, C. Han, G. Zhang, D. D. Dionysiou and M. N. Nadagouda, *Chem. Eng. J.*, 2015, **268**, 170–179.

211 F. Wang, J. Jiu, L. Pei, K. Nakagawa, S. Isoda and M. Adachi, *Chem. Lett.*, 2005, **34**, 418–419.

212 C. Hu, X. Zhang, W. Li, Y. Yan, G. Xi, H. Yang, J. Li and H. Bai, *J. Mater. Chem. A*, 2014, **2**, 2040–2043.

213 Z. Sun, J. H. Kim, Y. Zhao, F. Bijarbooneh, V. Malgras, Y. Lee, Y. Kang and S. X. Dou, *J. Am. Chem. Soc.*, 2011, **133**, 19314–19317.

214 H. Liu, T. Liu, X. Dong and Z. Zhu, *Mater. Lett.*, 2014, **134**, 240–243.

215 T. Balaganapathi, B. Kaniamuthan, S. Vinoth and P. Thilakan, *Mater. Chem. Phys.*, 2017, **189**, 50–55.

216 N. Asim, S. Radiman, M. A. Yarmo and M. S. Banaye Golriz, *Microporous Mesoporous Mater.*, 2009, **120**, 397–401.

217 Y. Dai, Q. Li, S. Tan, Q. Wei, Y. Pan, X. Tian, K. Zhao, X. Xu, Q. An, L. Mai and Q. Zhang, *Nano Energy*, 2017, **40**, 73–81.

218 S. L. Chou, J. Z. Wang, J. Z. Sun, D. Wexler, M. Forsyth, H. K. Liu, D. R. MacFarlane and S. X. Dou, *Chem. Mater.*, 2008, **20**, 7044–7051.

219 C. V. Subba Reddy, E. H. Walker, S. A. Wicker, Q. L. Williams and R. R. Kalluru, *Curr. Appl. Phys.*, 2009, **9**, 1195–1198.

220 L. Mai, Q. Wei, Q. An, X. Tian, Y. Zhao, X. Xu, L. Xu, L. Chang and Q. Zhang, *Adv. Mater.*, 2013, **25**, 2969–2973.

221 T. Puangpetch, S. Chavadej and T. Sreethawong, *Powder Technol.*, 2011, **208**, 37–41.

222 B. Saravanakumar, S. Maruthamuthu, V. Umadevi and V. Saravanan, *Int. J. Nanosci.*, 2018, **17**, 1–10.

223 A. M. Cao, J. S. Hu, H. P. Liang and L. J. Wan, *Angew. Chem., Int. Ed.*, 2005, **44**, 4391–4395.

224 B. Hu, H. Cheng, C. Huang, M. K. Aslam, L. Liu, C. Xu, P. Chen, D. Yu and C. Chen, *Solid State Ionics*, 2019, **342**, 115059.

225 S. Zhang, Y. Li, C. Wu, F. Zheng and Y. Xie, *J. Phys. Chem. C*, 2009, **113**, 15058–15067.

226 K. Panigrahi, P. Howli and K. K. Chattopadhyay, *Electrochim. Acta*, 2020, **337**, 135701.

227 M. Parthibavarman, M. Karthik and S. Prabhakaran, *Vacuum*, 2018, **155**, 224–232.

228 C. Y. Ng, K. A. Razak, A. A. Aziz and Z. Lockman, *J. Exp. Nanosci.*, 2014, **9**, 9–16.

229 L. M. Bertus, C. Faure, A. Danine, C. Labrugere, G. Campet, A. Rougier and A. Duta, *Mater. Chem. Phys.*, 2013, **140**, 49–59.

230 M. Aslam, I. M. I. Ismail, S. Chandrasekaran and A. Hameed, *J. Hazard. Mater.*, 2014, **276**, 120–128.

231 S. S. Mehta, M. S. Tamboli, I. S. Mulla and S. S. Suryavanshi, *J. Solid State Chem.*, 2018, **258**, 256–263.

232 S. Cao and H. Chen, *J. Alloys Compd.*, 2017, **702**, 644–648.

233 M. H. Wang, F. Zhou and B. Zhang, *Mater. Lett.*, 2014, **114**, 84–87.

234 H. Wang, M. Li, L. Jia, L. Li, G. Wang, Y. Zhang and G. Li, *Nanoscale Res. Lett.*, 2010, **5**, 1102–1106.

235 S. Bai, X. Liu, D. Li, S. Chen, R. Luo and A. Chen, *Sens. Actuators, B*, 2011, **153**, 110–116.

236 M. Amanullah, Q. ul A. Javed and S. Rizwan, *Mater. Chem. Phys.*, 2016, **180**, 128–134.

237 M. R. Parra and F. Z. Haque, *Optik*, 2015, **126**, 1562–1566.

238 S. Zhao, Y. Shen, X. Yan, P. Zhou, Y. Yin, R. Lu, C. Han, B. Cui and D. Wei, *Sens. Actuators, B*, 2019, **286**, 501–511.

239 C. Liangyuan, L. Zhiyong, B. Shouli, Z. Kewei, L. Dianqing, C. Aifan and C. C. Liu, *Sens. Actuators, B*, 2010, **143**, 620–628.

240 J. Li, G. Lu, Y. Wang, Y. Guo and Y. Guo, *J. Colloid Interface Sci.*, 2012, **377**, 191–196.

241 S. Ghosh, D. Majumder, A. Sen and S. Roy, *Mater. Lett.*, 2014, **130**, 215–217.

242 M. Zare, K. Namratha, K. Byrappa, D. M. Surendra, S. Yallappa and B. Hungund, *J. Mater. Sci. Technol.*, 2018, **34**, 1035–1043.

243 Y. T. Prabhu, K. V. Rao, V. S. S. Kumar and B. S. Kumari, *Adv. Nanopart.*, 2013, **02**, 45–50.

244 H. Hu, C. Deng and X. Huang, *Mater. Chem. Phys.*, 2010, **121**, 364–369.

245 X. L. Xu, Y. Chen, S. Y. Ma, S. H. Yan, Y. Z. Mao, T. Wang and H. Q. Bian, *Mater. Lett.*, 2015, **151**, 5–8.

246 Y. Miao, H. Zhang, S. Yuan, Z. Jiao and X. Zhu, *J. Colloid Interface Sci.*, 2016, **462**, 9–18.

247 X. Wang, A. Sumboja, E. Khoo, C. Yan and P. S. Lee, *J. Phys. Chem. C*, 2012, **116**, 4930–4935.

248 N. M. Dang, W. W. Zhao, S. I. Yusa, H. Noguchi and K. Nakashima, *New J. Chem.*, 2015, **39**, 4726–4730.

249 N. Dahal, I. A. Ibarra and S. M. Humphrey, *J. Mater. Chem.*, 2012, **22**, 12675–12681.

250 M. Pudukudy and Z. Yaakob, *Chem. Pap.*, 2014, **68**, 1087–1096.

251 J. Yang, M. Gao, J. Lei, X. Jin, L. Yu and F. Ren, *J. Solid State Chem.*, 2019, **274**, 124–133.

252 Y. Shang, D. Zhang and L. Guo, *J. Mater. Chem.*, 2012, **22**, 856–861.

253 M. M. Alam, W. Zhao, S. Zhai, S. I. Yusa, H. Noguchi and K. Nakashima, *Chem. Lett.*, 2014, **43**, 1426–1428.

254 R. Srivastava, M. U. Anu Prathap and R. Kore, *Colloids Surf., A*, 2011, **392**, 271–282.

255 X. Chang, G. Ji, K. Shen, L. Pan, Y. Shi and Y. Zheng, *J. Alloys Compd.*, 2009, **482**, 240–245.

256 T. Ghoshal, T. Maity, J. F. Godsell, S. Roy and M. A. Morris, *Adv. Mater.*, 2012, **24**, 2390–2397.

257 B. Y. Yu and S. Y. Kwak, *J. Mater. Chem.*, 2010, **20**, 8320–8328.

258 X. F. Qu, Q. Z. Yao, G. T. Zhou, S. Q. Fu and J. L. Huang, *J. Phys. Chem. C*, 2010, **114**, 8734–8740.

259 X. Pang, Y. He, J. Jung and Z. Lin, *Science*, 2016, **353**, 1268–1272.

260 T. Brezesinski, M. Groenewolt, M. Antonietti and B. Smarsly, *Angew. Chem., Int. Ed.*, 2006, **45**, 781–784.

261 C. Ye, K. Hu, Z. Niu, Y. Lu, L. Zhang and K. Yan, *J. Water Process. Eng.*, 2019, **27**, 205–210.

262 Z. Ai, K. Deng, Q. Wan, L. Zhang and S. Lee, *J. Phys. Chem. C*, 2010, **114**, 6237–6242.

263 P. K. Nayak and N. Munichandraiah, *Mater. Sci. Eng., B*, 2012, **177**, 849–854.

264 L. He, G. Zhang, Y. Dong, Z. Zhang, S. Xue and X. Jiang, *Nano-Micro Lett.*, 2014, **6**, 38–45.

265 C. Du, J. Yun, R. K. Dumas, X. Yuan, K. Liu, N. D. Browning and N. Pan, *Acta Mater.*, 2008, **56**, 3516–3522.

266 Y. Xia, Z. Qiang, B. Lee, M. L. Becker and B. D. Vogt, *CrystEngComm*, 2017, **19**, 4294–4303.

267 P. Wang, Y. Zhao, L. Wen, J. Chen and Z. Lei, *Ind. Eng. Chem. Res.*, 2014, **53**, 20116–20123.

268 J. Ma, Q. Cheng, V. Pavlinek, N. Stingelin and C. Silva, *New J. Chem.*, 2013, **37**, 722–728.

269 J. Liu, M. Sasidharan, D. Liu, Y. Yokoyama, S. I. Yusa and K. Nakashima, *Mater. Lett.*, 2012, **66**, 25–28.

270 B. P. Bastakoti, M. Imura, Y. Nemoto and Y. Yamauchi, *Chem. Commun.*, 2012, **48**, 12091–12093.

271 S. Chatterjee, R. Maiti, M. Miah, S. K. Saha and D. Chakravorty, *ACS Omega*, 2017, **2**, 283–289.

272 J. Massin, M. Bräutigam, N. Kaeffer, N. Queyriaux, M. J. Field, F. H. Schacher, J. Popp, M. Chavarot-Kerlidou, B. Dietzek and V. Artero, *Interface Focus*, 2015, **5**, 1–10.

273 J. Yin, Q. Xu, Z. Wang, X. Yao and Y. Wang, *J. Mater. Chem. C*, 2013, **1**, 1029–1036.

274 K. T. Lim, H. S. Hwang, W. Ryoo and K. P. Johnston, *Langmuir*, 2004, **20**, 2466–2471.

275 Y. Liu, R. Che, G. Chen, J. Fan, Z. Sun, Z. Wu, M. Wang, B. Li, J. Wei, Y. Wei, G. Wang, G. Guan, A. A. Elzatahry, A. A. Bagabas, A. M. Al-Enizi, Y. Deng, H. Peng and D. Zhao, *Sci. Adv.*, 2015, **1**, 1–8.

276 M. S. Seo, I. Jeong, J. S. Park, J. Lee, I. K. Han, W. I. Lee, H. J. Son, B. H. Sohn and M. J. Ko, *Nanoscale*, 2016, **8**, 11472–11479.

277 C. C. Weng, K. F. Hsu and K. H. Wei, *Chem. Mater.*, 2004, **16**, 4080–4086.

278 S. Zhan, D. Chen, X. Jiao and C. Tao, *J. Phys. Chem. B*, 2006, **110**, 11199–11204.

279 J. Yang, Y. L. Jiang, L. J. Li, E. Muhire and M. Z. Gao, *Nanoscale*, 2016, **8**, 8170–8177.

280 M. Gong, Y. Li, Y. Guo, X. Lv and X. Dou, *Sens. Actuators, B*, 2018, **262**, 350–358.

281 L. Sheng, T. Liao, L. Kou and Z. Sun, *Mater. Today Energy*, 2017, **3**, 32–39.

282 Z. Sun, J. H. Kim, Y. Zhao, F. Bijarbooneh, V. Malgras and S. X. Dou, *J. Mater. Chem.*, 2012, **22**, 11711–11719.

283 J. Li, Q. L. Zhao, G. Y. Zhang, J. Z. Chen, L. Zhong, L. Li, J. Huang and Z. Ma, *Solid State Sci.*, 2010, **12**, 1393–1398.

284 C. Cummins, A. P. Bell and M. A. Morris, *Nanomaterials*, 2017, **7**, 1–12.

285 Z. Wang, D. Wang and J. Sun, *Sens. Actuators, B*, 2017, **245**, 828–834.

286 Y. Liang, Y. Yang, C. Zou, K. Xu, X. Luo, T. Luo, J. Li, Q. Yang, P. Shi and C. Yuan, *J. Alloys Compd.*, 2019, **783**, 848–854.

287 A. Yan, C. Xie, D. Zeng, S. Cai and H. Li, *J. Alloys Compd.*, 2010, **495**, 88–92.

288 D. Xu, K. Ge, S. Qi, Y. Chen, J. Qiu, S. Wang, Y. Tian, S. Fang, C. Liu and Q. Liu, *J. Mater. Sci.*, 2020, **55**, 7645–7651.

289 B. A. Çakir, L. Budama, Ö. Topel and N. Hoda, *Colloids Surf., A*, 2012, **414**, 132–139.

290 C. H. Braun, T. V. Richter, F. Schacher, A. H. E. Müller, E. J. W. Crossland and S. Ludwigs, *Macromol. Rapid Commun.*, 2010, **31**, 729–734.

291 X. Li, W. Dou and N. Bao, *Mater. Lett.*, 2012, **68**, 140–142.

292 P. Amornpitoksuk, S. Suwanboon, S. Sangkanu, A. Sukhoom, J. Wudtipan, K. Srijan and S. Kaewtaro, *Powder Technol.*, 2011, **212**, 432–438.

293 P. Amornpitoksuk, S. Suwanboon, S. Sangkanu, A. Sukhoom and N. Muensit, *Superlattices Microstruct.*, 2012, **51**, 103–113.

294 Y. H. Jang, S. Y. Yang, Y. J. Jang, C. Park, J. K. Kim and D. H. Kim, *Chem. – Eur. J.*, 2011, **17**, 2068–2076.

295 H. Zhang, R. Wu, Z. Chen, G. Liu, Z. Zhang and Z. Jiao, *CrystEngComm*, 2012, **14**, 1775–1782.

296 G. Liu, F. He, X. Li, S. Wang, L. Li, G. Zuo, Y. Huang and Y. Wan, *J. Mater. Chem.*, 2011, **21**, 10637–10640.

297 R. A. Soomro, Z. H. Ibupoto, Sirajuddin, M. I. Abro and M. Willander, *Sens. Actuators, B*, 2015, **209**, 966–974.

298 F. E. Atalay, D. Asma, H. Kaya, A. Bingol and P. Yaya, *Nanomater. Nanotechnol.*, 2016, **6**, 1–6.

299 C. Yu, X. Li, Z. Liu, X. Yang, Y. Huang, J. Lin, J. Zhang and C. Tang, *Mater. Res. Bull.*, 2016, **83**, 609–614.

300 X. Chen, D. H. Kuo and D. Lu, *Chem. Eng. J.*, 2016, **295**, 192–200.

301 S. Bolisetty, J. Adamcik, J. Heier and R. Mezzenga, *Adv. Funct. Mater.*, 2012, **22**, 3424–3428.

302 N. Talavera, M. Navarro, A. A. Boada-sucre and I. Gonzalez, *Recent Res. Dev. Mater. Sci.*, 2013, **10**, 89–102.

303 D. Ramimoghadam, M. Z. Bin Hussein and Y. H. Taufiq-Yap, *Chem. Cent. J.*, 2013, **7**, 1–10.

304 X. L. Cheng, J. Sen Jiang, C. Y. Jin, C. C. Lin, Y. Zeng and Q. H. Zhang, *Chem. Eng. J.*, 2014, **236**, 139–148.

305 S. R. Patil, B. H. Hameed, A. S. Škapin and U. L. Štangar, *Chem. Eng. J.*, 2011, **174**, 190–198.

306 M. P. Rao, S. Anandan, S. Suresh, A. M. Asiri and J. J. Wu, *Energy Environ. Focus*, 2015, **4**, 250–255.